Directional stability assessment of a wingsail-driven vessel

MT54035: MSc Thesis

Guido Haenen

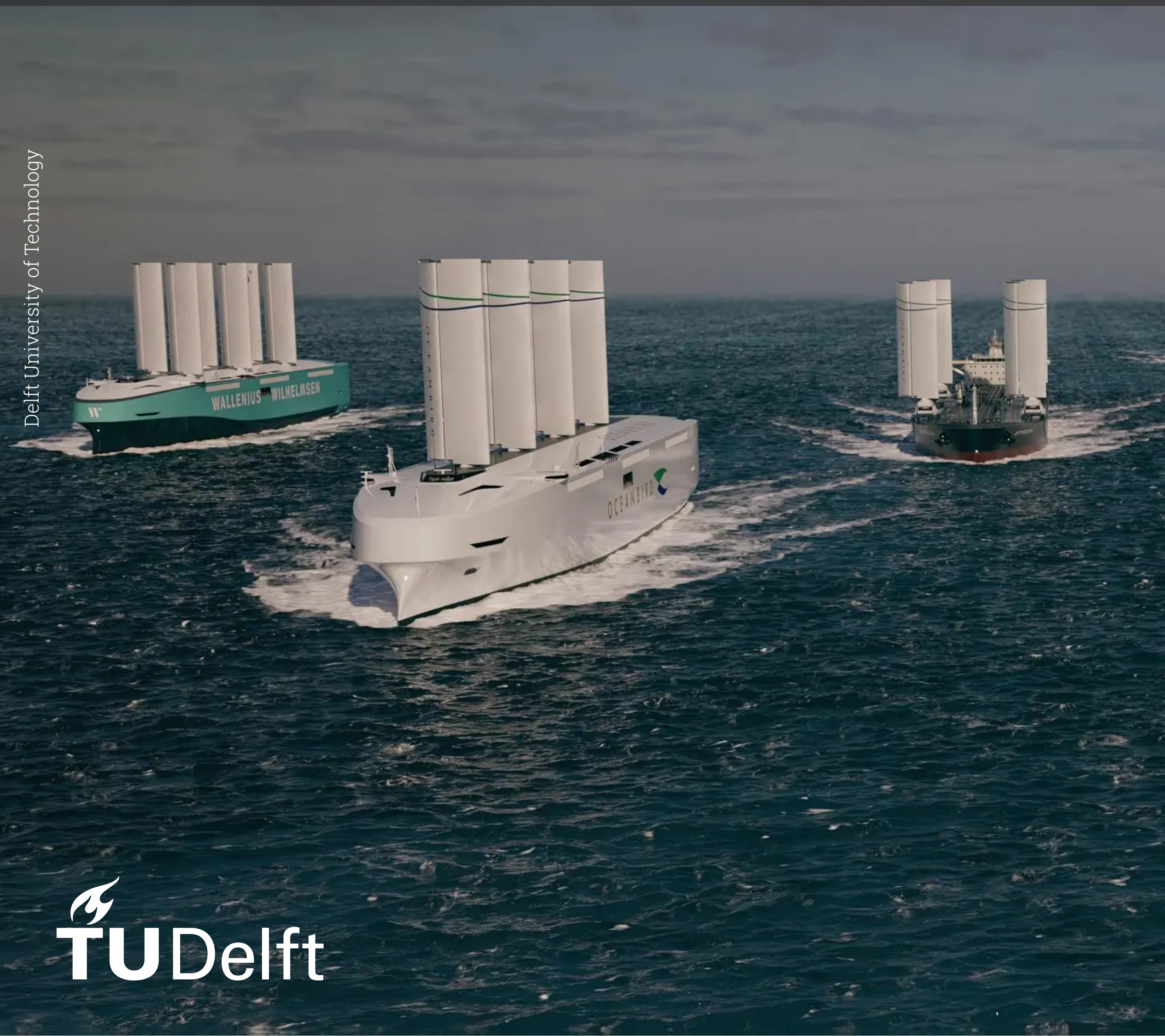

Delft University of Technology

Directional stability assessment of a wingsail-driven vessel

by

Guido Haenen

performed at

RISE Research Institutes of Sweden

to obtain the degree of Master of Science in Marine Technology

in the specialisations of Marine Engineering, Ship Hydromechanics and Ship Design

at the Delft University of Technology,

to be defended publicly on Friday September 6, 2024 at 09:00.

Main supervisor:	Andrea Coraddu	a.
Company supervisor 1:	Fredrik Olsson	
Company supervisor 2:	Martin Alexandersson	
Student number:	4398602	
Thesis number:	MT23/24.047M	
Project duration:	8 December 2024 – 6 September 2024	
Thesis committee:	Dr. A. Coraddu,	TU Delft
	Dr. ir. P. de Vos,	TU Delft
	Dr. ir. A. Rijkens,	TU Delft
	N. Vasilikis,	TU Delft
	M. Alexandersson,	RISE SSPA

Cover:	Artist impression of Orcelle Wind by Oceanbird (Modified)
Style:	TU Delft Report Style, with modifications by Daan Zwaneveld

Preface

Dear Reader,
This report marks the culmination of nine months of work on the Oceanbird car carrier, completed as part of my master's thesis in Marine Technology.

I would like to express my sincere gratitude to Fredrik Olsson, my industry supervisor, for giving me the opportunity to undertake this thesis at RISE SSPA. Your initial ideas helped shape the direction of this research and our weekly meetings were invaluable. I greatly appreciated the engineering contexts you provided, which served as an essential counterbalance to the mathematical focus of the problem.

I also extend my thanks to Andrea Coraddu for your unwavering support and flexibility throughout this process. Your ability to instil confidence in me and to provide efficient, helpful, and insightful feedback on my progress was truly admirable.

I am very grateful to Martin Alexandersson for his expertise in manoeuvring theory and his meticulous attention to detail. Your time and effort in helping me refine this report have been incredibly beneficial.

Lastly, I want to thank my friends and family for their constant support and belief in me.

Guido Haenen
Amsterdam, August 2024

Abstract

This thesis investigates the yaw stability of wind-driven vessels using wingsails, addressing the urgent need for decarbonising global shipping. An analytical method is developed to assess directional stability based on aerodynamic and hydrodynamic characteristics, yielding a universal stability criterion validated with SEAMAN data. The study explores practical stability assessment approaches and evaluates the impact of varying hydrodynamic parameters, aerodynamic models, and surge coupling effects.

Results show that while stability diagnostics are invariant under different hydrodynamic models, significant variations occur in destabilised hulls. Including a boundary layer in the wind model has negligible effects on stability but increases computational effort. The closed-loop analysis assesses proportional and derivative feedback control strategies, demonstrating satisfactory stability for both human and autopilot control across all points of sail in the original hull configuration.

Time-domain responses to step rudder inputs indicate small steady errors and oscillatory components under human control, with autopilot control yielding even more robust outcomes. The study highlights the importance of surge coupling in stability analysis, often overlooked in previous models. The thesis concludes that wind-driven vessels can achieve directional stability under active control schemes, providing a foundation for future research on sustainable maritime transportation.

Contents

Preface ii

Abstract iv

Nomenclature vii

1 Introduction 1

2 Methodology 3
2.1 Approach 3
2.1.1 Model assumptions 4
2.2 Force Model 5
2.2.1 Hydrodynamic forces 7
2.2.2 Aerodynamic superstructure forces 8
2.2.3 Sail forces 9
2.2.4 Stability formulation 9
2.3 VPP algorithm 10
2.4 Linearisation 11
2.4.1 Wind linearisation and superstructure 11
2.4.2 Sail forces 12
2.4.3 Hydrodynamics 14
2.4.4 Inertial forces 14
2.5 Stability assessment 15

3 Case Study 17

4 Results 23
4.1 Steady state results 23
4.2 Open-loop stability assessment 23
4.3 Modelling approaches 27
4.3.1 Wind flow model 27
4.3.2 Surge coupling 27
4.4 Closed-loop analysis 28
4.5 Yaw motion 30

5 Conclusions 35
5.1 Analytical method 35
5.2 Model variations 35
5.3 Closed-loop analysis 36
5.4 Future work 36

References 38

A Intermediate VPP results 40

Nomenclature

Symbols

Symbol	Definition	Unit
A_S	Total sail area	[m]
A_T	Projected transverse hull area	[m]
B	Ship beam	[m]
C_D	Drag coefficient	[-]
C_L	Lift coefficient	[-]
h_B	Sail base height measured from waterline	[m]
h_S	Total sail height measured from sail base	[m]
I_z	Moment of inertia around z-axis	[kg·m^2]
k_{zz}	Radius of gyration around z-axis	[m]
L	Ship length	[m]
l_C	Chord length	[m]
m	Mass	[kg]
N	Moment in yaw direction	[N·m]
r	Yaw velocity	[rad/s]
s_i	Sheeting angle at the i^{th} sail	[rad]
T	Ship draft	[m]
TWA	True wind direction relative to ship velocity	[rad]
u	Surge velocity	[m/s]
U	Total ship velocity	[m/s]
v	Sway velocity	[m/s]
V_{10m}	True wind speed at $z = 10$m	[m/s]
V_A	Apparent wind speed	[m/s]
V_T	Local true wind speed	[m/s]
X	Forces in surge direction	[N]
Y	Forces in sway direction	[N]
x_g	Longitudinal centre of mass position	[m]
α	Angle of attack	[rad]
β	Drift angle	[rad]
δ	Rudder angle	[rad]
θ_A	Apparent wind direction relative to bow	[rad]
θ_W	True wind direction relative to bow	[rad]
ρ	Water density	[kg/m^3]
ρ_a	Air density	[kg/m^3]
ψ	Yaw angle	[rad]
∇	Ship displacement	[m^3]

1 Introduction

Climate change poses a significant threat to human well-being and planetary health [3]. A critical measure to mitigate its impact is the rapid decarbonisation of the global economy. One sector contributing notably to carbon emissions is shipping, accounting for approximately 3% of total annual anthropogenic CO2 emissions [5]. The International Maritime Organisation (IMO) aims to reduce total annual GHG emissions from international shipping by at least 20% (striving for 30%) by 2030 and by at least 70% (striving for 80%) by 2040, compared to 2008 levels. Additionally, carbon intensity should be reduced by at least 40% by 2030 [10].

Achieving these ambitious targets presents significant challenges for the global shipping industry. Policymakers play a crucial role in regulating fossil fuel supply and demand, incorporating climate change externalities into fuel prices, and addressing the Jevons paradox by reducing shipping volumes. However, the engineering science community must focus on understanding and overcoming technical challenges to enhance transport efficiency.

Although numerous solutions exist, the most effective and straightforward approach—reducing transport volumes—is politically sensitive and beyond the scope of this research. Operational strategies to improve transport efficiency include just-in-time arrival, minimum time in port, weather routing, slow steaming, trim optimization, autopilot improvements, better fleet and cargo management, ballast optimization, hull roughness reduction, and propeller maintenance, upgrade, and optimization [19]. Design and retrofit options involve alternative fuels, carbon capture and storage, engine optimization, waste heat recycling, space optimization, autonomous shipping, installation of energy-saving devices, direct environmental propulsion assistance, and wind propulsion.

Wind propulsion, in particular, remains a promising candidate for decarbonizing both new ships and refits due to its historically proven effectiveness. However, fully wind-driven vessels face operational and financial limitations that hinder their competitiveness with traditional cargo fleets under current fossil-favoring fiscal policies. Despite these challenges, the scientific and societal interest in wind propulsion has grown rapidly.

Traditionally, wind-driven vessels harness wind power through on-deck devices such as (wing)sails, Flettner rotors, or kites, which generate a net force opposite to the vessel's bow. This method introduces a side force component, causing the vessel to sail at a drift angle. The nonlinear nature of hull hydrodynamics in large commercial vessels renders classical straight-line stability criteria ([4][1]) unreliable for predicting directional stability under drift conditions. Therefore, a generalised analytical stability criterion that accounts for wind forces is necessary.

Previous research has partially addressed this gap by extending analytical stability criteria to include steady wind conditions [6][20][23][2]. Notably, the work of [25][26] represents a significant step towards understanding stability in steady wind scenarios and proposes a generalisation of the classical stability criterion.

However, wind forces on wind-driven vessels significantly influence surge forces (which were deemed insignificant by [25]), necessitating further investigation into factors affecting directional stability in cargo vessels driven solely by wingsails. This area remains relatively unexplored due to the novelty of wind propulsion in large vessels compared to the well-studied stability of sailing yachts with slender hulls.

To address these gaps, this thesis explores the following research questions:

To what extent is a vessel able to maintain yaw stability under the influence of varying wind conditions and control system specifications when introducing large aerodynamic control surfaces?

1. Which analytical methods can be used to assess the directional stability of vessels equipped with large aerodynamic control surfaces?
2. How do different modelling approaches impact the directional stability assessment of vessels?
3. How does the yaw motion of the system behave in both the frequency domain and the time domain under proportional and derivative feedback control strategies?

By investigating these questions, this research aims to contribute to the development of effective solutions for achieving yaw stability in wind-driven vessels under varying wind conditions and control system specifications.

2 Methodology

2.1. Approach

When answering the respective research questions, care should be taken that the obtained results are as generally applicable as possible. That said, while developing the methodology, a specific test case of a wind-powered car carrier (wPCC) with four wingsails placed on the centre line was analysed. This is especially relevant for the aerodynamic characteristics, which in general differs depending on the vessel. However, since the aerodynamic part is considered as a separate module and interaction effects are disregarded, the end result should be general with respect to arbitrary aerodynamic models.

When approaching the question of developing an analytical methodology for assessing directional stability, an important starting point is to define directional stability. Stability is a concept which relates to dynamical systems, which is the study of the time evolution of points that belong to a certain mathematical space, or more specifically, a vector space, as is usually the case in engineering contexts. This step means therefore to choose the particular vector space that is relevant to the problem at hand.

To that effect, a mathematical force model first needs to be crystallised which then leads to a concrete (simplified) description of the relevant motions that relate to directional stability. The model simplifications and limitations should be made clear, which helps defining the model itself as well as charting possible directions for future work. The model should also be sufficiently accurately describe the dynamics of the vessel. In essence this part comes down to describing the forces acting on a rigid body, since hydroelasticity can be assumed negligible in a manoeuvring context [23].

After developing the forces that act on the vessel, a steady state or force equilibrium can be found if the environmental conditions are known (wind speed and wind direction). Finding these steady states means optimising for speed while keeping the drift angle, the rudder angle, and the angles of attack of the sails within certain constraints. This step therefore reduces to a constrained optimisation problem, for which an algorithm will be described. It is also known as a Velocity Prediction Programme (VPP).

Stability of a point is defined by properties of a small neighbourhood around the point in question. Therefore, linearisation of the forces is another piece of the puzzle, and although this step in theory only constitutes simple higher-dimensional differentiation, i.e. writing out Jacobian matrices, the tricky part lies in unpacking the expressions until they are written in terms of parameters and variables that are considered to be known.

Finally, the notion of stability of a steady state is explored through an equivalent criterion called the Routh-Hurwitz criterion, which is a particularly useful tool in stability theory since it gives information about the roots of the characteristic polynomial of a differential equation which is useful for determining stability, without actually having to know the numerical value of the roots. This is particularly powerful since by the Abel-Ruffini theorem, roots of polynomials of at least order 5 can in general not be written in terms of their coefficients. Although in this thesis, at most order 4 polynomials will be considered, this fact is of possible relevance to more complex force models, for example, with more degrees of freedom.

To apply the methodology to an actual test vessel and obtain numerical results, all of the symbolic parameters and variables must be resolved. The force model depends on physical constants (e.g. water and air density), independent variables (wind speed and direction), and case-specific parameters. The case parameters generally refer to the dimensions of the ship, the centre of mass, the rigging layout, the hydrodynamic coefficients (including the rudder), the lift and drag characteristics of the wingsails, and the drag coefficients of the superstructure. Depending on the amount of analysis performed on a particular vessel, sometimes these parameters are already known. In other cases, semi-empirical methods or educated guesses are needed.

The most important dependent variable resulting from the methods described above is something that can be most aptly described as the “degree of instability” of the system. This boils down to the maximum of the real parts of the eigenvalues of the state transition matrix of the system, and its sign determines whether the whole system is stable or not. The parameter can be interpreted as a diagnostic value which mostly gives binary information (stable/unstable), although its magnitude is also indicative of how close the system is to being marginally stable.

In order to solidify confidence in the developed stability assessment, several modelling choices are varied and the effect on the results of the case study are examined. This forms the heart of the second subquestion.

Finally, the closed-loop effects are studied when introducing proportional and derivative gain in the system, and the step response in the time domain is analytically solved for a few specific operational conditions. This constitutes the answer to the third subquestion.

2.1.1. Model assumptions

The forces on the vessel can be divided into inertia forces, hydrodynamic forces, and aerodynamic forces. An additional subdivision can then be made for the hydrodynamic forces into hull forces, rudder forces, and possibly propeller forces, depending on additional simplifications that the analytical calculations may warrant. A possible simplification is to assume that the propeller rate is adjusted according to the required forward speed, yielding a constant forward speed as the thrust and extra wind resistance cancel out. The aerodynamic forces can be subdivided into the forces exerted on the superstructure by the wind, and the forces experienced by the wingsail system, which can be controlled. Consequently, the reaction forces (inertial pseudoforces, hull forces and superstructure forces) can be grouped together, while the control forces (rudder and sail system) can be grouped together as well.
A priori all six degrees of freedom of the ship are relevant when considering a realistic situation for a vessel on sea. However, in many modelling situations, one or more of the ship motions may be constrained in order to simplify the mechanics, provided that the simplifying assumptions are reasonable in the case considered. Alternatively, other simplifying assumptions can be made with respect to environmental forces or other forces. In this case, a 3DOF model is considered (surge, sway and yaw).
The assumptions that will be made are the following:

- Deep-water conditions may be assumed, i.e. water depth is modelled as infinite;
- There is no interference from other vessels, shores or other objects;
- Fluid memory effects are ignored, i.e. a quasi-static approach is taken;
- The ship hull is considered rigid, which means hydro-elasticity is assumed negligible;
- All control surfaces are considered rigid;
- Calm water is assumed, i.e. no wave excitation is considered;
- The wind profile is considered uniform in space and time and no interaction effects between the different sails are considered;
- Roll is assumed negligible.

Whether or not roll motions may be considered negligible is an interesting question, and it can be expected that the answer in general is negative, particularly when it comes to more extreme weather conditions. However, for most cargo vessels, a roll angle of 5° is already considered rather extreme and the captain will generally reduce the sail area in order to avoid heeling too much. In practice the maximum heel angle will be limited to about 5 degrees. That said, some non-negligible roll-sway-yaw-rudder couplings may occur even at small heel angles, generally introducing instabilities into the system. The extent to which this occurs is influenced by the drift angle as well [13]. A paper on nonlinear stability of ship autopilots by Fossen and Lauvdal suggests a minimal speed to maintain controllability when designing a combined yaw autopilot and rudder-roll stabilisation system [8]. An experimental study on two different RoRo vessels suggests that the linear derivatives N_v' and N_r' may change by respectively $+20\%$ and -25% for a heel angle of $5°$ [9]. A sensitivity study on a particular container ship (S175), based on a nonlinear 4DOF steering model by Son and Nomoto, concludes that there are several roll-dependent hydrodynamic derivatives that have a moderate or moderate to high effect on the manoeuvring characteristics of the vessel in question [18]. Ship manoeuvrability may be significantly influenced by trim and loading condition as well [11]. However, for the purposes of simplification it is chosen to focus on the three most important degrees of freedom and to leave out the effects of trim and loading condition, as well as any shallow water effects that could influence manoeuvrability.

2.2. Force Model

In this section, a force model will be developed that serves as the basis for all calculations, both for the steady-state solutions and for the stability evaluations. Various conventions exist concerning how equations of motion should be written down. In this thesis, a control theory approach will be taken insofar as the notation will strive towards a state-space formulation.

In this thesis, a 3-DOF force model is used. The motions and forces considered are in the surge, sway, and yaw direction. The most important shortcoming of such a model is its limited applicability for stronger winds, as the heeling forces and consequent heeling motions will not be negligible in such conditions. Using Newton's laws of motion, the relation between accelerations and forces is given. The relation between generalised velocity and forces is given by empirical tests from the literature. The goal is to describe the dynamics of the system in a state-space representation.

The first goal is to describe the dynamics of a fully sailing cargo vessel with four sails and one rudder using a modular force model. This means the total accelerations on the vessel will be given by the sum of the forces and pseudoforces (due to a non-inertial reference frame) on the various components of the ship. An inertial NED frame (North-East-Down) and a ship-fixed body frame are defined as described in [7]. In the ship coordinate system, the origin is in the midship, while the centre of mass is in the centreline of the ship, at distance x_g in the x-direction. The coordinate frames are shown in Figure 2.1.

Forces will be expressed in the ship body frame so that the hydrodynamic forces become more straightforward than would otherwise be the case. However, since the ship frame is not inertial, this means that several pseudo-forces like Coriolis and centripetal forces will be introduced that would not appear in an inertial frame. The dynamic equations follow from Newton's laws as well as basic calculus and are documented in [7]:

$$\begin{cases} m(\dot{u} - vr - x_g r^2) & = \sum X \\ m(\dot{v} - ur - x_g \dot{r}) & = \sum Y \\ (I_z + m x_g^2)\dot{r} + m x_g(\dot{v} + ur) & = \sum N \end{cases} \tag{2.1}$$

Here the sums on the right-hand side constitute all external forces acting on the ship. Note that the moment of inertia I_z is defined with respect to the centre of mass, which gives rise to a term mx_g^2 resulting from the Parallel Axis Theorem.

The terms on the left-hand side containing velocities can be grouped and moved to the right-hand side. They will be called inertial pseudo-forces:

$$\mathbf{F}_{I,RB} := \begin{bmatrix} m(vr + x_g r^2) \\ -mur \\ -m x_g ur \end{bmatrix} \tag{2.2}$$

The point is to group the acceleration terms on the left-hand side and all other terms on the right-hand side. This gives rise to the following vector $\mathbf{F}_{RB}$:

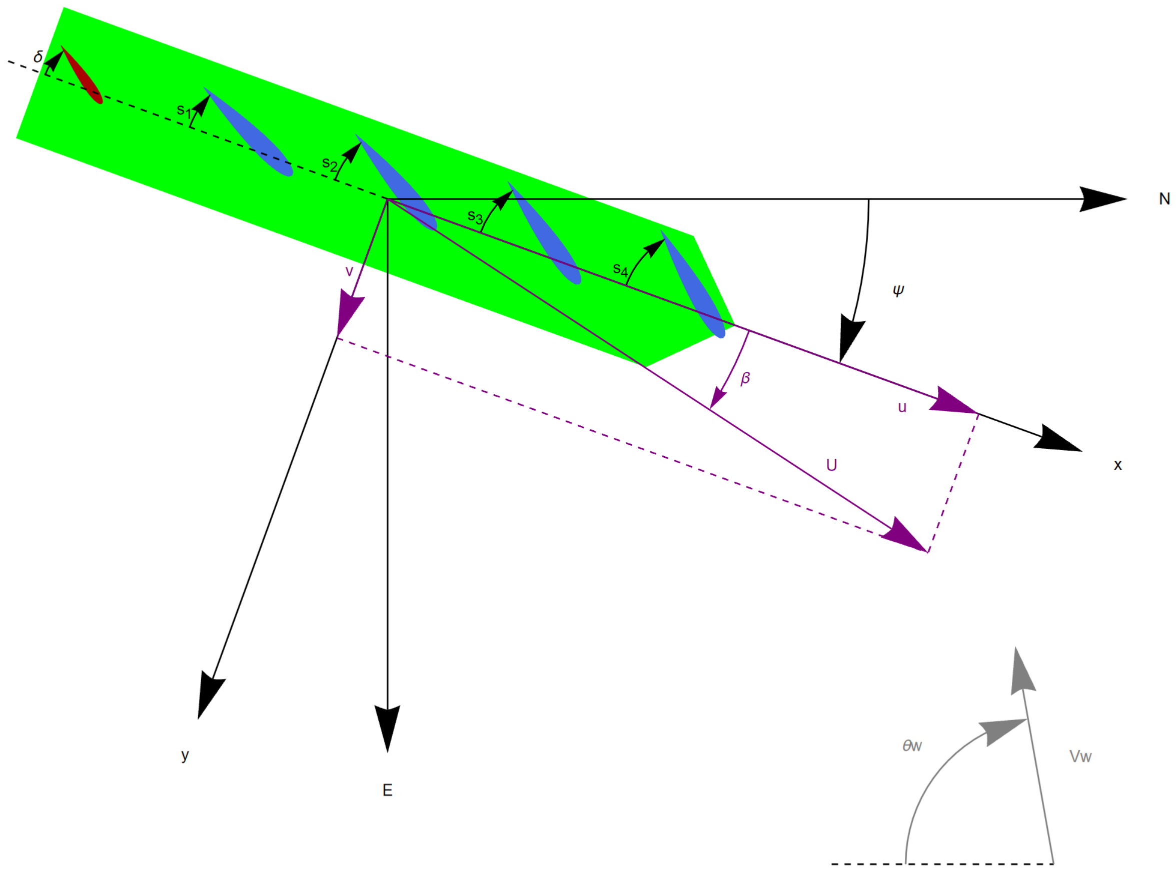

Figure 2.1: Coordinate system and sign conventions

$$\mathbf{F}_{RB} = \begin{bmatrix} X_{RB} \\ Y_{RB} \\ N_{RB} \end{bmatrix} := \begin{bmatrix} m(vr + x_g r^2) + \sum X \\ -mur + \sum Y \\ -mx_g ur + \sum N \end{bmatrix} = \mathbf{F}_{I,RB} + \mathbf{F}_H + \mathbf{F}_A + \mathbf{F}_S \tag{2.3}$$

The force vectors $\mathbf{F}_H, \mathbf{F}_A$, and $\mathbf{F}_S$, are the hydrodynamic hull forces (including rudder forces), aerodynamic forces acting on the ship superstructure, and the sail forces, respectively. These will be elaborated upon in the following sections. The acceleration terms of Equation 2.1 give rise to the following definition:

$$\mathbf{M}_{RB} := \begin{bmatrix} m & 0 & 0 \\ 0 & m & mx_g \\ 0 & mx_g & I_z + mx_g^2 \end{bmatrix} \tag{2.4}$$

The velocities in 3 degrees of freedom are written as ν:

$$\nu := \begin{bmatrix} u \\ v \\ r \end{bmatrix} \tag{2.5}$$

Following Equations 2.1,2.3,2.4, and 2.5, the equations of motion can then be rewritten as follows:

$$\mathbf{M}_{RB}\dot{\nu} = \mathbf{F}_{RB} \tag{2.6}$$

2.2.1. Hydrodynamic forces

The hydrodynamic forces can be subdivided in potential forces, inertial forces and manoeuvring forces:

$$\mathbf{F}_H = -\mathbf{M}_A\dot{\nu} + \mathbf{F}_{I,A} + \mathbf{F}_{man}, \tag{2.7}$$

where each term will be explained below. The latter two terms can be combined, as we will see.

The added masses constitute the extra hydrodynamic forces that result from accelerating the water around the vessel and are a direct result of Newton's third law. The hydrodynamic forces due to this phenomenon are called potential forces. Here we model the off-diagonal added masses as zero:

$$\mathbf{M}_A\dot{\nu} = -\begin{bmatrix} X_{\dot{u}} & 0 & 0 \\ 0 & Y_{\dot{v}} & 0 \\ 0 & 0 & N_{\dot{r}} \end{bmatrix} \begin{bmatrix} \dot{u} \\ \dot{v} \\ \dot{r} \end{bmatrix} \tag{2.8}$$

It is worth elaborating on the Munk moment. Potential flow theory gives us an expression for the magnitude of the Munk moment in terms of the added masses of the body. The forces as a result of the change in kinetic energy of the surrounding fluid take a rather similar form as the inertial forces described in Equation 2.2, and depend on the added masses of the ship. Sagatun and Fossen [17] constructed the concept of a Coriolis and centripetal matrix $\mathbf{C}_A$ for the added masses, based on the Kirchhoff equations. This matrix contains, besides some minor adjustments to the force matrix by Davidson and Schiff [4], the more significant Munk moment that is not explicitly included in many manoeuvring models. These forces are defined as follows:

$$\mathbf{F}'_{I,A} = \mathbf{C}'_A \begin{bmatrix} u' \\ v' \\ r' \end{bmatrix} = \begin{bmatrix} -Y'_{\dot{v}}v'r' - Y'_{\dot{r}}r'^2 \\ X'_{\dot{u}}u'r' \\ (Y'_{\dot{v}} - X'_{\dot{u}})u'v' + Y'_{\dot{r}}u'r' \end{bmatrix}. \tag{2.9}$$

In Equation 2.9, all primed parameters and variables mean that the respective quantities are nondimensionalised according to the Prime System - specifically, the Prime System I which doesn't use draft as a reference quantity but only length. Since in our force model, only the hydrodynamic forces result from a nondimensional framework, the choice was made to convert those forces to SI values and then calculate all results in a dimensional setting. This choice is all the more valid since usually, but not in our case, ship velocity is kept constant, which warrants its use as a reference speed. For more information on nondimensionalisation, see Section $7.2.5$ from [7]. All of the above forces become zero in the pure translation case $r = 0$, except for the term $(Y_{\dot{v}} - X_{\dot{u}})uv$, which is known as the Munk moment.

However, the hull forces $\mathbf{F}_{man}$ also depend on ν. Many different manoeuvring models can be chosen to model these, and the choice of such a model is a very interesting topic of discussion, although outside of the scope of this thesis. In this case, a polynomial model was adopted that has the following form:

$$X'_H = X'_0 + X'_u u' + X'_{vv} v'^2 + X'_{vr} v' r' + X'_{rr} r'^2 + X'_{\delta\delta}\delta^2 \tag{2.10}$$

$$\begin{aligned} Y'_H = {} & Y'_v v' + Y'_r r' + Y'_{vvv} v'^3 + Y'_{vvr} v'^2 r' + Y'_{vrr} v' r'^2 + Y'_{rrr} r'^3 + Y'_\delta \delta \\ & + Y'_{\delta\delta\delta}\delta^3 + Y'_{r\delta\delta} r'\delta^2 + Y'_{rr\delta} r'^2\delta + Y'_{v\delta\delta} v'\delta^2 + Y'_{vv\delta} v'^2\delta + Y'_{vr\delta} v' r'\delta \end{aligned} \tag{2.11}$$

$$\begin{aligned} N'_H = {} & N'_v v' + N'_r r' + N'_{vvv} v'^3 + N'_{vvr} v'^2 r' + N'_{vrr} v' r'^2 + N'_{rrr} r'^3 + N'_\delta \delta \\ & + N'_{\delta\delta\delta}\delta^3 + N'_{r\delta\delta} r'\delta^2 + N'_{rr\delta} r'^2\delta + N'_{v\delta\delta} v'\delta^2 + N'_{vv\delta} v'^2\delta + N'_{vr\delta} v' r'\delta \end{aligned} \tag{2.12}$$

Since the total moment acting on the ship due to pure translation is a combination of both the Munk moment arising from potential theory and the viscous force contribution, there is no real advantage in including the potential terms explicitly (see also the discussion by Sutulo and Soares on this matter [21]). This holds not only for the Munk moment but also for the other terms present in $\mathbf{F}_{I,A}$, although they are comparatively less significant in magnitude. Hence, for manoeuvring modelling purposes, the added mass Coriolis and centripetal forces can be included in the hull forces. The attentive reader will note that in the above manoeuvring model, terms like N'_{ur} are missing, which would seemingly render the previous argument invalid. However, in the linearised model, this caveat disappears, since $X_{\dot{u}} u_0$ can then be included in N'_v or N'_{vvv}, and the other terms in $\mathbf{F}_{I,A}$ can be treated similarly. The polynomial model is less physical in the sense that the individual terms contain blurred physical information, and the fitting is done over the whole model. However, it works well enough for most simple purposes. Summarising all of the above, for the purposes of this thesis, $\mathbf{F}_{I,A} = 0$.

Combining all of the above with Equation 2.6 and defining $\mathbf{M} := \mathbf{M}_{RB} + \mathbf{M}_A$ gives us the final force equation and a force vector called $\mathbf{F}_{tot}$ containing various forces and pseudoforces:

$$\mathbf{M}\dot{\nu} = \mathbf{F}_{RB} + \mathbf{M}_A\dot{\nu} = \mathbf{F}_{I,RB} + \mathbf{F}_{man} + \mathbf{F}_A + \mathbf{F}_S =: \mathbf{F}_{tot} \tag{2.13}$$

2.2.2. Aerodynamic superstructure forces

The aerodynamic forces $\mathbf{F}_A$ experienced by the superstructure of the ship are related to the speed of the ship at a reference point (in this case the origin of the ship frame), also called the apparent wind. The model used is the following:

$$\mathbf{F}_A = \begin{bmatrix} X_A \\ Y_A \\ N_A \end{bmatrix} = \frac{1}{2}\rho_a V_A^2 \begin{bmatrix} A_T C_X(\theta_A) \\ A_T C_Y(\theta_A) \\ L A_T C_N(\theta_A) \end{bmatrix} \tag{2.14}$$

where ρ_a is the density of air, V_A is the apparent wind speed at the origin, and A_T is the transverse projected area of the superstructure. Note that sometimes the lateral projected area A_L is used as a reference area for Y_A and N_A, but this is just a convention issue and in the case study of this thesis, only the coefficients with respect to A_T were given. Lastly, C_X, C_Y and C_N are empirically determined force coefficients that depend on the shape of the hull and vary with the apparent wind angle θ_A.

If the true wind $(u_T, v_T)^T$ at a certain point (x, y, z) is known, as well as the ship speeds (u, v, r), the apparent wind at that point can be calculated by

$$\begin{bmatrix} u_A \\ v_A \end{bmatrix} = \begin{bmatrix} u - yr + u_T(z) \\ v + xr + v_T(z) \end{bmatrix} \tag{2.15}$$

$$\theta_A = \operatorname{atan2}(u_A, v_A) \tag{2.16}$$

$$V_A^2 = u_A^2 + v_A^2 = (u - yr + u_T(z))^2 + (v + xr + v_T(z))^2 \tag{2.17}$$

where the true wind $(u_T, v_T)^T$ is obtained by applying a rotation transformation as it both depends on the wind direction and the ship orientation (see Figure 2.1):

$$\begin{bmatrix} u_T \\ v_T \end{bmatrix} = \mathbf{R}(\theta_w - \psi) \begin{bmatrix} V_T \\ 0 \end{bmatrix} = \begin{bmatrix} V_T \cos(\theta_W - \psi) \\ V_T \sin(\theta_W - \psi) \end{bmatrix} \tag{2.18}$$

The wind speed is modelled with the atmospheric boundary layer and will therefore vary in magnitude depending on the height above the surface:

$$V_T(z) = V_{10m} \left(\frac{-z}{10\,\mathrm{m}} \right)^{1/7} \tag{2.19}$$

Note that because of the right-handed coordinate system, a minus appears in the numerator. The forces $\mathbf{F}_A$ are modelled to always act at a height of $10\,\mathrm{m}$, hence the effective wind speed for $\mathbf{F}_A$ will be equal to V_{10m}. In the next section, we will see in more detail how the boundary layer affects the sails.

2.2.3. Sail forces

The sail forces depend on ship speed, true wind, orientation, and sheeting angles. For any nonzero ship speed, the boundary layer will cause variations in both the magnitude and direction of the apparent wind as a function of height. This “twist effect” is well known to operators of sailing vessels, usually dealt with by shaping the sail such that the sheeting angle becomes larger in the top part of the sail. In the case of a rigid sail, this is impossible and the twist effect will result in a varying angle of attack profile along the height.

The wind is assumed to exert only forces and no yaw moments on the sails. As a result, the yaw moment delivered by the sails is solely due to the side forces multiplied by the respective force arms. The thrust and side forces experienced by a single sail are obtained by a coordinate transformation from the drag and lift forces. These are defined as, respectively, the force component aligned with the flow and the component perpendicular to the flow. The relation to thrust and side force is then given by

$$\begin{bmatrix} f_T(z) \\ f_S(z) \end{bmatrix} = \mathbf{R}(\pi + \theta_A(z)) \begin{bmatrix} f_D(z) \\ f_L(z) \end{bmatrix} = \begin{bmatrix} -\cos(\theta_A(z)) & \sin(\theta_A(z)) \\ -\sin(\theta_A(z)) & -\cos(\theta_A(z)) \end{bmatrix} \begin{bmatrix} f_D(z) \\ f_L(z) \end{bmatrix} \tag{2.20}$$

where f_T, f_S, f_D and f_L are the force *densities* of the sail as a function of local angle of attack. The total forces exerted on the sail are given by

$$\begin{bmatrix} F_T \\ F_S \end{bmatrix} = \int_{z=-h_b}^{-(h_b+h_S)} \begin{bmatrix} f_T(z) \\ f_S(z) \end{bmatrix} dz \tag{2.21}$$

while the drag and lift force densities themselves are modelled as follows:

$$\begin{bmatrix} f_D(z) \\ f_L(z) \end{bmatrix} = \frac{1}{2} \rho_a V_A(z)^2 L_c(z) \begin{bmatrix} C_D(\alpha(z)) \\ C_L(\alpha(z)) \end{bmatrix} \tag{2.22}$$

where $L_c(z)$ is the local chord length of the sail (varying with height) and $\alpha(z) = \theta_A(z) - s$ is the angle of attack, defined as the difference between the apparent wind angle θ_A and the sheeting angle s. The lift and drag coefficients of a rigid sail as functions of the angle of attack are considered known.

Finally, the forces exerted on all sails together make up the total sail forces, where $m \in \mathbb{N}$ is the number of sails and x_{r_i} is the x position of sail number i (which constitutes the lever arm for the moment delivered by that sail):

$$\begin{bmatrix} X_S \\ Y_S \\ N_S \end{bmatrix} = \sum_{i=1}^{m} \begin{bmatrix} 1 & 0 \\ 0 & 1 \\ 0 & x_{r_i} \end{bmatrix} \begin{bmatrix} F_{T_i} \\ F_{S_i} \end{bmatrix} \tag{2.23}$$

2.2.4. Stability formulation

Course stability can be described as the tendency for the yaw angle to restore to the equilibrium value after a disturbance. To say something meaningful about stability, an equilibrium has to be found first.

This is generally done through a velocity prediction programme (VPP). Using the force model as described in the rest of this section, a simplified VPP was constructed to find the approximate operational points of the ship in full sailing mode. A steady-state solution will have a constant yaw angle ψ_0. This angle can be assumed equal to zero without loss of generality because we can align the inertial coordinate system with the bow direction in the steady state. This means that in general, the inertial reference frame is not a literal North-East-Down frame anymore, but as this thesis does not deal with navigational factors, this is not a problem. Furthermore, for the steady state, the yaw rate $r_0 = 0$ since $r = \dot{\psi} = 0$ by definition of steady state. The total steady state solution $\mathbf{x}_0$ will hence consist of velocities u_0 and v_0 in the horizontal plane, a steady rudder angle δ_0 and steady sheeting angles $s_{1,0}, \dots, s_{4,0}$.

Using control theory notation, the stability problem can be described by a state-space description, defining

$$\mathbf{x} := \begin{bmatrix} \Delta u \\ \Delta v \\ r \\ \psi \end{bmatrix} = \begin{bmatrix} u - u_0 \\ v - v_0 \\ r \\ \psi \end{bmatrix} \tag{2.24}$$

as the state. The state evolution matrix $\mathbf{A}$ will describe how the state changes as a function of itself. Another matrix $\mathbf{B}$ describes the state change as a function of inputs $\mathbf{u}$, which are defined as the physical quantities that are directly adjustable by the controller. The state-space representation then takes the following form:

$$\dot{\mathbf{x}} = \mathbf{A}\mathbf{x} + \mathbf{B}\mathbf{u} \tag{2.25}$$

Note that the steady term vanished due to the definition of $\mathbf{x}$ as the unsteady part of the variables u, v, r, ψ. Higher-order terms are also not written here, although they will be present in general. However, if all relevant functions are smooth enough with bounded derivatives, then Taylor's theorem guarantees a linear approximation provided $\mathbf{x}$ and $\mathbf{u}$ are small enough. However, as the model is highly nonlinear, the linearisations $\mathbf{A}$ and $\mathbf{B}$ depend on the steady state $\mathbf{x}_0, \mathbf{u}_0$.

In a simple control model, we can choose $\Delta\delta$ and $\Delta s_1, \dots, \Delta s_4$ as input variables, whereas, in a real situation, both the rudder and the sheeting angle are subject to their own dynamics. In such more precise models, the input variables would in extreme examples be given by the duty ratio of the chopper inside the sheeting actuator. For this model, the rudder and sheets are assumed to be directly controllable:

$$\mathbf{u} := \begin{bmatrix} \Delta\delta \\ \Delta s_1 \\ \Delta s_2 \\ \Delta s_3 \\ \Delta s_4 \end{bmatrix} = \begin{bmatrix} \delta - \delta_0 \\ s_1 - s_{1,0} \\ s_2 - s_{2,0} \\ s_3 - s_{3,0} \\ s_4 - s_{4,0} \end{bmatrix} \tag{2.26}$$

Like stated earlier, the workflow of the open-loop stability evaluation at a certain wind speed V_{10m} and wind angle θ_w consists of the following steps:

- Developing a force model and choosing environmental conditions (V_{10m}, θ_w);
- Solving a constrained optimisation problem to find the associated operational point $\mathbf{x}_0, \mathbf{u}_0$;
- Computing stability derivatives of all forces at the operational point;
- Evaluating the Hurwitz stability of the associated state transition matrix.

2.3. VPP algorithm

Finding the steady state associated with a certain environmental condition is akin to solving the following constrained optimisation problem:

$$\begin{aligned} &\text{minimise } -(u_0^2 + v_0^2) \\ &\text{subject to} \\ &\mathbf{F}_{tot}(u_0, v_0, \delta_0, s_{1,0}, \dots, s_{4,0}) = \mathbf{0}, \\ &g(u_0, v_0, \delta_0, s_{1,0}, \dots, s_{4,0}) \leq \mathbf{0}. \end{aligned}$$

The equality constraint means that the steady state should be a force equilibrium. The inequality constraint imposes boundaries on the decision variables $u_0, v_0, \delta_0, s_{1,0}, \dots, s_{4,0}$ by enforcing positive forward velocity and limits on the drift angle $\beta_0 := \operatorname{atan2}(u_0, v_0)$, rudder angle δ_0 and angles of attack $\alpha_{i,0} := \theta_A(x_{r_i}, 0, -h_b) - s_{i,0}$, measured at the foot of the sails. The following limits were used:

$$\begin{cases} u_0 \geq 0; \\ \beta_0 \in [-10°, 10°]; \\ \delta_0 \in [-35°, 35°]; \\ \alpha_{i,0} \in [-20°, 20°]. \end{cases} \tag{2.27}$$

To solve this optimisation problem, a Sequential Quadratic Programming (SQP) algorithm was used, which is an iterative method for solving nonlinear constrained optimisation problems. The core of the algorithm consists of expanding the dimension of the objective space by a Lagrange multipliers for all active constraints, then approximating the Lagrangian function by a positive definite Hessian matrix. This is also called a Lagrange-Newton method. Specialised techniques called quasi-Newton methods exist to make sure the matrix is both positive definite and approximates the Hessian of the Lagrangian well enough, although for the purposes of this thesis, starting from a close enough guess turned out to suffice for positive-definiteness and for letting the algorithm converge without resorting to sophisticated methods. The so-called QP subproblem is an unconstrained convex optimisation problem and hence has a guaranteed solution. This solution defines a search direction from the last guess, after which a line search is performed to find the next guess. When certain convergence criteria are satisfied for the constraints and the objective function, or when a maximum number of iterations is performed, the algorithm concludes. For more details regarding the exact algorithm, page 314 from [16] may be consulted.

2.4. Linearisation

In this section, the forces acting on the vessel are differentiated so that the state transition matrix can be found. Suppose for a start that a steady state $\mathbf{x}_0 = (u_0, v_0, r_0 = 0, \psi_0 = 0)^T$ is found. Then let $\varepsilon > 0$ and let $(\Delta u, \Delta v, r, \psi) = \mathcal{O}(\varepsilon)$ be a perturbation vector (heuristically, a vector “close enough” to zero to ensure that all linearisations approximate the original functions sufficiently).

2.4.1. Wind linearisation and superstructure

First, the apparent wind speed, which appears in both the superstructure wind forces (Equation 2.14) and the sail forces (Equation 2.22) will be treated. Its linearisation around a certain value V_{A0} is as follows (following notation also used in [25] and expanding it):

$$V_A^2 = V_{A0} + V_{Au}\Delta u + V_{Av}\Delta v + V_{Ar} r + V_{A\psi}\psi + \mathcal{O}(\varepsilon^2) \tag{2.28}$$

for any $(\Delta u, \Delta v, r, \psi)^T \in \mathcal{O}(\varepsilon)$, with the coefficients given as

$$V_{A0} = (u_0 + V_T \cos\theta_W)^2 + (v_0 + V_T \sin\theta_W)^2 \tag{2.29}$$
$$V_{Au} = 2(u_0 + V_T \cos\theta_W) \tag{2.30}$$
$$V_{Av} = 2(v_0 + V_T \cos\theta_W) \tag{2.31}$$
$$V_{Ar} = 2x_{r_i}(v_0 + V_T \cos\theta_W) = x_{r_i} V_{Av} \tag{2.32}$$
$$V_{A\psi} = 2V_T(u_0 \sin\theta_W - v_0 \cos\theta_W) \tag{2.33}$$

In the above equations, V_T is the local true wind speed (varying only with height above the free surface) and θ_W is the true wind direction measured from the bow of the ship. The apparent wind angle can be linearised as follows, using similar terminology as in [25] but including also the effect of yaw rate in the apparent wind:

$$\theta_A = \theta_{A0} + \theta_{Au}\Delta u + \theta_{Av}\Delta v + \theta_{Ar} r + \theta_{A\psi}\psi + \mathcal{O}(\varepsilon^2) \tag{2.34}$$

with the following expressions specifying the linear sensitivities of the apparent wind angle to the various state variables:

$$\theta_{A0} = \tan^{-1}\left(\frac{v_0 + V_T \sin\theta_W}{u_0 + V_T \cos\theta_W}\right) \tag{2.35}$$

$$\theta_{Au} = -\frac{v_0 + V_T \sin\theta_W}{V_{A0}} \tag{2.36}$$

$$\theta_{Av} = \frac{u_0 + V_T \cos\theta_W}{V_{A0}} \tag{2.37}$$

$$\theta_{Ar} = x_{r_i}\frac{u_0 + V_T \cos\theta_W}{V_{A0}} = x_{r_i}\theta_{Av} \tag{2.38}$$

$$\theta_{A\psi} = -\frac{V_T^2 + V_T(v_0 \sin\theta_W + u_0 \cos\theta_W)}{V_{A0}} \tag{2.39}$$

The superstructure is subject to wind forces as explained in the previous work by [6][20][25]:

$$\begin{bmatrix} X_A \\ Y_A \\ N_A \end{bmatrix} = \begin{bmatrix} X_{A0} \\ Y_{A0} \\ N_{A0} \end{bmatrix} + \begin{bmatrix} X_{Au} & X_{Av} & 0 & X_{A\psi} \\ Y_{Au} & Y_{Av} & 0 & Y_{A\psi} \\ N_{Au} & N_{Av} & 0 & N_{A\psi} \end{bmatrix} \begin{bmatrix} \Delta u \\ \Delta v \\ r \\ \psi \end{bmatrix} + \mathcal{O}(\varepsilon^2) \tag{2.40}$$

with the steady-state forces given by

$$\begin{bmatrix} X_{A0} \\ Y_{A0} \\ N_{A0} \end{bmatrix} = \frac{1}{2}\rho_a V_{A0} \begin{bmatrix} A_X C_{XA}(\theta_{A0}) \\ A_Y C_{YA}(\theta_{A0}) \\ A_Y L C_{NA}(\theta_{A0}) \end{bmatrix} \tag{2.41}$$

and the “aerodynamic derivatives” as follows:

$$X_{Ai} = \frac{1}{2}\rho_a A_X \left(V_{A0}\frac{\partial C_{XA}(\theta_{A0})}{\partial\theta_A}\theta_{Ai} + V_{Ai}C_{XA}(\theta_{A0})\right) \tag{2.42}$$

$$Y_{Ai} = \frac{1}{2}\rho_a A_Y \left(V_{A0}\frac{\partial C_{YA}(\theta_{A0})}{\partial\theta_A}\theta_{Ai} + V_{Ai}C_{YA}(\theta_{A0})\right) \tag{2.43}$$

$$N_{Ai} = \frac{1}{2}\rho_a A_Y L \left(V_{A0}\frac{\partial C_{NA}(\theta_{A0})}{\partial\theta_A}\theta_{Ai} + V_{Ai}C_{NA}(\theta_{A0})\right) \tag{2.44}$$

for $i = u, v, \psi$.

2.4.2. Sail forces

For the sails, the linearisation is considerably more involved. The linear derivatives which will constitute the entries of the Jacobian matrix $\mathrm{D}_{\mathbf{x}}\mathbf{F}_S$ of the sail forces are denoted by the subscript S, hence giving rise to the following notation:

$$\mathbf{F}_S = \mathbf{F}_{S0} + (\mathrm{D}_{\mathbf{x}}\mathbf{F}_S)\Delta\mathbf{x} + \mathcal{O}(\varepsilon^2) = \begin{bmatrix} X_S \\ Y_S \\ N_S \end{bmatrix} = \begin{bmatrix} X_{S0} \\ Y_{S0} \\ N_{S0} \end{bmatrix} + \begin{bmatrix} X_{Su} & X_{Sv} & X_{Sr} & X_{S\psi} \\ Y_{Su} & Y_{Sv} & Y_{Sr} & Y_{S\psi} \\ N_{Su} & N_{Sv} & N_{Sr} & N_{S\psi} \end{bmatrix} \begin{bmatrix} \Delta u \\ \Delta v \\ r \\ \psi \end{bmatrix} + \mathcal{O}(\varepsilon^2) \tag{2.45}$$

Note that contrary to the simpler superstructure wind force model, a nonzero yawing rate dependence is present in the model, since the sails (especially the outermost ones) will experience varying apparent wind speeds when the ship is yawing.

The above Jacobian matrix is itself a linear combination of the derivatives of the forces on the individual sails:

$$\mathrm{D}_{\mathbf{x}}\mathbf{F}_S = \begin{bmatrix} 1 & 0 & 1 & 0 & \cdots & 1 & 0 \\ 0 & 1 & 0 & 1 & \cdots & 0 & 1 \\ 0 & x_{r_1} & 0 & x_{r_2} & \cdots & 0 & x_{r_m} \end{bmatrix} \begin{bmatrix} \frac{\partial F_{T_1}}{\partial u} & \frac{\partial F_{T_1}}{\partial v} & \frac{\partial F_{T_1}}{\partial r} & \frac{\partial F_{T_1}}{\partial \psi} \\ \frac{\partial F_{S_1}}{\partial u} & \frac{\partial F_{S_1}}{\partial v} & \frac{\partial F_{S_1}}{\partial r} & \frac{\partial F_{S_1}}{\partial \psi} \\ \vdots & \vdots & \vdots & \vdots \\ \frac{\partial F_{T_m}}{\partial u} & \frac{\partial F_{T_m}}{\partial v} & \frac{\partial F_{T_1}}{\partial r} & \frac{\partial F_{T_1}}{\partial \psi} \\ \frac{\partial F_{S_m}}{\partial u} & \frac{\partial F_{S_m}}{\partial v} & \frac{\partial F_{S_m}}{\partial r} & \frac{\partial F_{S_m}}{\partial \psi} \end{bmatrix} \tag{2.46}$$

where the force derivatives $\frac{\partial F_{T_i}}{\partial u}, \frac{\partial F_{S_i}}{\partial u} \ldots, \frac{\partial F_{T_i}}{\partial \psi}, \frac{\partial F_{S_i}}{\partial \psi}$ in turn are given by differentiating the thrust and side forces of the respective sail:

$$\begin{aligned} \begin{bmatrix} \frac{\partial F_{T_1}}{\partial u} & \frac{\partial F_{T_1}}{\partial v} & \frac{\partial F_{T_1}}{\partial r} & \frac{\partial F_{T_1}}{\partial \psi} \\ \frac{\partial F_{S_1}}{\partial u} & \frac{\partial F_{S_1}}{\partial v} & \frac{\partial F_{S_1}}{\partial r} & \frac{\partial F_{S_1}}{\partial \psi} \end{bmatrix} &= \frac{\partial}{\partial \mathbf{x}} \int_{z=-h_b}^{-(h_b+h_S)} \frac{1}{2}\rho_a V_A^2(z) \mathbf{R}(\theta_A(z)+\pi) \begin{bmatrix} C_D(\alpha(z)) \\ C_L(\alpha(z)) \end{bmatrix} dz \\ &= \frac{1}{2}\rho_a \int_{z=-h_b}^{-(h_b+h_S)} \frac{\partial}{\partial \mathbf{x}} \left(V_A^2(z) \mathbf{R}(\theta_A(z)+\pi) \begin{bmatrix} C_D(\alpha(z)) \\ C_L(\alpha(z)) \end{bmatrix} \right) dz \\ &= \frac{1}{2}\rho_a \int_{z=-h_b}^{-(h_b+h_S)} \left(\mathbf{R}(\theta_A(z)+\pi) \begin{bmatrix} C_D(\alpha(z)) \\ C_L(\alpha(z)) \end{bmatrix} \right) \frac{\partial}{\partial \mathbf{x}} (V_A^2(z)) \\ &\quad + \frac{\partial}{\partial \mathbf{x}} (\mathbf{R}(\theta_A(z)+\pi) \left(V_A^2(z) \begin{bmatrix} C_D(\alpha(z)) \\ C_L(\alpha(z)) \end{bmatrix} \right) \\ &\quad + \left(V_A^2(z) \mathbf{R}(\theta_A(z)+\pi) \right) \frac{\partial}{\partial \mathbf{x}} \left(\begin{bmatrix} C_D(\alpha(z)) \\ C_L(\alpha(z)) \end{bmatrix} \right) dz \end{aligned} \tag{2.47}$$

where it should be kept in mind that this rather cumbersome expression is the result of standard calculus applications like the product rule and the appropriate switching of integral and derivative (which is always allowed when the functions are smooth enough - hence the later choice for continuously differentiable splines).

The right lid of Equation 2.47 can be developed even further. The first term contains the factor $\frac{\partial}{\partial \mathbf{x}}(V_A^2(z))$, which is equal to $\begin{bmatrix} V_{Au} & V_{Av} & V_{Ar} & V_{A\psi} \end{bmatrix}$ calculated with respect to the wind speed at height z. The third term contains $\frac{\partial}{\partial \mathbf{x}} \left(\begin{bmatrix} C_D(\alpha(z)) \\ C_L(\alpha(z)) \end{bmatrix} \right)$ which, by the definition $\alpha(z) = s - \theta_A(z)$ is equal to

$$-\begin{bmatrix} \frac{\partial C_D}{\partial \alpha} \\ \frac{\partial C_L}{\partial \alpha} \end{bmatrix} \begin{bmatrix} \theta_{Au} & \theta_{Av} & \theta_{Ar} & \theta_{A\psi} \end{bmatrix}.$$

This is the part where the derivatives of the drag and lift coefficients of the sails need to be known. The second term from Equation 2.47 contains terms that ultimately all relate back to the apparent wind angle θ_A and its linearisation.

The upshot is that the state variable $\mathbf{x}$ influences the force density at a certain sail section in three different ways:

- Through the apparent wind speed;
- Through the change in direction of the flow, which has an effect on the rotation matrix;
- Through the change in direction of the flow, which indirectly influences the drag and lift coefficients because the angle of attack changes.

The first of these effects was already mentioned before when analysing the aerodynamic forces on the superstructure and the aerodynamic derivatives $V_{Au}, \ldots, V_{A\psi}$. The second effect requires calculating the derivative of the rotation matrix, which is just a phase offset of $\frac{\pi}{2}$. The third effect requires knowledge of (the first derivative of) the drag and lift coefficient functions. In the example case, these are just low-degree polynomials, of which the derivative becomes relatively simple. It should be noted that in a realistic wind-propelled scenario, the wingsails will make use of the drag profile in following wind conditions, which means that values of α beyond the stall angle will appear. Such a scenario will entail additional modelling complexity due to turbulence patterns that need high-fidelity sail-sail interactions in the model. Therefore angles beyond stall are not considered here and α will be limited to at most $20°$.

Lastly, the methodology described above holds in general for flow models with a nonuniform boundary layer like the one described in Equation 2.19, but just as well for the uniform flow model of $V_T(z) \equiv V_{10m}$. In the latter case, the integral over the sail height can be resolved before making the actual calculations, thereby greatly reducing computational effort.

2.4.3. Hydrodynamics

The hydrodynamic forces are linearised as follows (note that the yaw angle ψ is unrelated to the hydrodynamic forces):

$$\mathbf{F}_H = \mathbf{F}_{H0} + (\mathrm{D}_\mathbf{x}\mathbf{F}_H)\Delta\mathbf{x} + \mathcal{O}(\varepsilon^2) = \begin{bmatrix} X_{H0} \\ Y_{H0} \\ N_{H0} \end{bmatrix} + \begin{bmatrix} X_{Hu} & X_{Hv} & X_{Hr} & 0 \\ Y_{Hu} & Y_{Hv} & Y_{Hr} & 0 \\ N_{Hu} & N_{Hv} & N_{Hr} & 0 \end{bmatrix} \begin{bmatrix} \Delta u \\ \Delta v \\ r \\ \psi \end{bmatrix} + \mathcal{O}(\varepsilon^2) \tag{2.48}$$

The hydrodynamic derivatives are originally defined in a dimensionless vector space where it becomes relatively easy to relate a small perturbation from the steady state to a specific term like Y'_v, N'_r or similar. This is the way it worked with the original stability criterion. However, as stated also elsewhere, the fact that in this case wind also has a substantial effect on the surge forces and hence on the total ship speed by virtue of acting on a sail vessel, makes the choice for a coordinate system which is nondimensionalised by the vessel speed $U = \sqrt{u^2 + v^2}$ unnatural. The total derivative of the hydrodynamic forces will therefore be a lot messier than in other literature about manoeuvring theory, since the simplification of having a constant ship speed during manoeuvring is unwarranted and actually, terms like $\frac{\partial U}{\partial u}, \ldots, \frac{\partial U}{\partial]psi}$ are also part of the full expression.

Two immediate attempts at solving come to mind. The first is to fit sea trials and model tests to a polynomial model which uses dimensional speeds and do all actual calculations in SI units. However, since $\sqrt{u^2 + v^2}$ is not a polynomial itself, the result will be a model of which the polynomial coefficients will be hard to their nondimensional counterparts elsewhere in the literature. Nonetheless, this is the route that was chosen to perform the numerical calculations in the Results chapter. The other solution is to nondimensionalise the other forces and perform the whole linearisation and consequent stability analysis in nondimensional space. This is also not ideal on account of the fact that these forces will be divided by the ship speed . In other words, this solves the problem of unwieldy hydrodynamic forces but introduces the same problem for all the other forces.

The most elegant solution would be to make all variables nondimensional by a quantity that is invariant in the context of the problem at hand. Where the ship speed $\sqrt{u^2 + v^2}$ is useful for making quantities nondimensional in the context of manoeuvring problems that consider ship speed invariant, it is not so useful for our problem. Wind speed could be used, although it would lose its usefulness when examining the ship stability under fluctuating wind patterns. This might be a major qualitative problem when using high-fidelity models like the one from [12] while trying to verify stability resulting from an analytical which divides all values by the wind speed. Of course, in such a case, one might resort to using the mean wind speed instead, but the point stands that for all analytical methods, the constants really need to behave like constants in order for the method to be trustworthy.

2.4.4. Inertial forces

The inertial forces are linearised very easily. The observation that $r_0 = 0$ yields a very straightforward expression:

$$\begin{bmatrix} X_{Iu} & X_{Iv} & X_{Ir} & X_{I\psi} \\ Y_{Iu} & Y_{Iv} & Y_{Ir} & Y_{I\psi} \\ N_{Iu} & N_{Iv} & N_{Ir} & N_{I\psi} \end{bmatrix} = m \begin{bmatrix} 0 & 0 & v_0 & 0 \\ 0 & 0 & -u_0 & 0 \\ 0 & 0 & x_g u_0 & 0 \end{bmatrix} \tag{2.49}$$

In other words, the quadratic term $m x_g r^2$ is negligible around a non-rotating steady state. What remains is the $C_{RB}*$ matrix from [7], generalised for a nonzero side velocity.

2.5. Stability assessment

After obtaining a solution for the constrained optimisation problem, the force derivatives at that point can be computed. From now on, the term $\mathcal{O}(\varepsilon^2)$ will be dropped since it can be assumed that the perturbation from the steady state is small enough.

$$\mathrm{D}_{\mathbf{x}}\mathbf{F}_{tot} = \begin{bmatrix} X_{t,u} & X_{t,v} & X_{t,r} & X_{t,\psi} \\ Y_{t,u} & Y_{t,v} & Y_{t,r} & Y_{t,\psi} \\ N_{t,u} & N_{t,v} & N_{t,r} & N_{t,\psi} \end{bmatrix} = \begin{bmatrix} X_{Au} & X_{Av} & 0 & X_{A\psi} \\ Y_{Au} & Y_{Av} & 0 & Y_{A\psi} \\ N_{Au} & N_{Av} & 0 & N_{A\psi} \end{bmatrix} + \begin{bmatrix} X_{Su} & X_{Sv} & X_{Sr} & X_{S\psi} \\ Y_{Su} & Y_{Sv} & Y_{Sr} & Y_{S\psi} \\ N_{Su} & N_{Sv} & N_{Sr} & N_{S\psi} \end{bmatrix}$$
$$+ \begin{bmatrix} X_{Hu} & X_{Hv} & X_{Hr} & 0 \\ Y_{Hu} & Y_{Hv} & Y_{Hr} & 0 \\ N_{Hu} & N_{Hv} & N_{Hr} & 0 \end{bmatrix} + \begin{bmatrix} 0 & 0 & X_{Ir} & 0 \\ 0 & 0 & Y_{Ir} & 0 \\ 0 & 0 & N_{Ir} & 0 \end{bmatrix} \tag{2.50}$$

The steady state was a force equilibrium, therefore the total forces can be written as the product of the $\mathrm{D}_{\mathbf{x}}$ matrix and the state vector $(\Delta u, \Delta v, r, \psi)^T$. Also, this is the moment to invoke Equation 2.13 which related the forces to $(\dot{u}, \dot{v}, \dot{r})$.

$$\mathbf{M}\begin{bmatrix} \dot{u} \\ \dot{v} \\ \dot{r} \end{bmatrix} = \begin{bmatrix} X_{tot} \\ Y_{tot} \\ N_{tot} \end{bmatrix} = \mathrm{D}_{\mathbf{x}}\mathbf{F}_{tot}\begin{bmatrix} \Delta u \\ \Delta v \\ r \\ \psi \end{bmatrix} \tag{2.51}$$

From here, the state transition matrix $\mathbf{A}$ follows, which directly relates the time derivatives of the state to the state itself. A similar process also leads to the input matrix $\mathbf{B}$. This matrix can be built much like how the $\mathbf{A}$ matrix was constructed. The leftmost column will be closely related to some combination of the hydrodynamic parameters $X_{\delta\delta}$, Y_{δ},$N_{vr\delta}$, and the steady state speeds u_0 and v_0, while the other columns relate to the aerodynamic forces through the angle of attack $\alpha = s - \theta_A$.

$$\dot{\mathbf{x}} = \begin{bmatrix} \dot{u} \\ \dot{v} \\ \dot{r} \\ \dot{\psi} \end{bmatrix} = \overbrace{\begin{bmatrix} \mathbf{M}^{-1} \cdot \mathrm{D}_{\mathbf{x}}\mathbf{F}_{tot} \\ \hline 0 \quad 0 \quad 1 \quad 0 \end{bmatrix}}^{\mathbf{A}} \begin{bmatrix} \Delta u \\ \Delta v \\ r \\ \psi \end{bmatrix} + \overbrace{\begin{bmatrix} \mathbf{M}^{-1} \cdot \mathrm{D}_{\mathbf{u}}\mathbf{F}_{tot} \\ \hline \mathbf{0} \end{bmatrix}}^{\mathbf{B}} \begin{bmatrix} \Delta\delta \\ \Delta s_1 \\ \Delta s_2 \\ \Delta s_3 \\ \Delta s_4 \end{bmatrix} = \mathbf{Ax} + \mathbf{Bu} \tag{2.52}$$

The Jacobian of the steady-state solution needs to be determined to evaluate the stability of an ODE system. This is the state transition matrix $\mathbf{A}$. If one or more of its eigenvalues lie in the right half-plane, the corresponding eigenvector leads to an unstable solution. Therefore the problem reduces to analysing the roots of the characteristic equation of $\mathbf{A}$.

The characteristic polynomial of the state transition matrix $\mathbf{A}$ will be written as follows:

$$\mathrm{char}(\mathbf{A}) = a_0\lambda^4 + a_1\lambda^3 + a_2\lambda^2 + a_3\lambda + a_4 \tag{2.53}$$

Its coefficients can be calculated from the force matrix derivatives and the mass matrix and amount to the following (note that the entire monic polynomial was first multiplied by $\det(\mathbf{M})$ to obtain a simpler expression):

$$\begin{aligned}
a_0 &= \det(M); \\
a_1 &= -m_{11}m_{22}N_{t,r} + m_{11}m_{23}N_{t,v} + m_{11}m_{32}Y_{t,r} + m_{23}m_{32}X_{t,u} - m_{11}m_{33}Y_{t,v} - m_{22}m_{33}X_{t,u}; \\
a_2 &= m_{11}Y_{t,v}N_{t,r} - m_{22}X_{t,r}N_{t,u} + m_{22}X_{t,u}N_{t,r} - m_{11}m_{22}N_{t,\psi} + m_{23}X_{t,v}N_{t,u} - m_{23}X_{t,u}N_{t,v} \\
&\quad + m_{32}X_{t,r}Y_{t,u} + m_{11}m_{32}Y_{t,\psi} - m_11Y_{t,r}N_{t,v} - m_{32}X_{t,u}Y_{t,r} - m_{33}X_{t,v}Y_{t,u} + m_{33}X_{t,u}Yt,v; \\
a_3 &= X_{t,r}Y_{t,v}N_{t,u} - X_{t,v}Y_{t,r}N_{t,u} - X_{t,r}Y_{t,u}N_{t,v} + X_{t,u}Y_{t,r}N_{t,v} + X_{t,v}Y_{t,u}N_{t,r} - X_{t,u}Y_{t,v}N_{t,r} \\
&\quad - X_{t,u}Y_{t,\psi}N_{t,v} + m_{11}Y_{t,v}N_{t,\psi} - m_{22}X_{t,\psi}N_{t,u} + m_{22}X_{t,u}N_{t,\psi} + m_{32}X_{t,\psi}Y_{t,u} - m_{32}X_{t,u}Y_{t,\psi}; \\
a_4 &= X_{t,\psi}Y_{t,v}N_{t,u} + X_{t,u}Y_{t,\psi}N_{t,v} + X_{t,v}Y_{t,u}N_{t,\psi} - X_{t,v}Y_{t,\psi}N_{t,u} - X_{t,\psi}Y_{t,u}N_{t,v} - X_{t,u}Y_{t,v}N_{t,\psi}
\end{aligned}$$

By the Routh-Hurwitz criterion, the stability of $\mathrm{char}(\mathbf{A})$, which means the condition that all roots lie in the left half-plane, is equivalent to the following system of inequalities:

$$\Delta_0 = a_0 > 0; \tag{2.54}$$
$$\Delta_1 = a_1 > 0; \tag{2.55}$$
$$\Delta_2 = a_1 a_2 - a_0 a_3 > 0; \tag{2.56}$$
$$\Delta_3 = a_1 a_2 a_3 - a_0 a_3^2 - a_1^2 a_4 > 0; \tag{2.57}$$
$$\Delta_4 = a_4 > 0. \tag{2.58}$$

It should be noted that this condition is stronger than the condition that all $a_i > 0$. The system can be simplified by noting that a_0 is equal to the determinant of the mass matrix which means it will always be positive. Furthermore, a_1 is always positive since the force derivatives $X_{t,u}, Y_{t,v}, N_{t,r}$ are all negative, and the off-diagonal terms of the mass matrix are relatively small compared to the diagonal terms (provided the vessel has a center of mass reasonably close to the midship). The other Hurwitz coefficients $\Delta_2, \Delta_3, \Delta_4$ are less straightforward in terms of predicting their signs in a general setting. All of the previous derivations can be summarised in the following statement:

The vessel is (open-loop) stable if and only if $\Delta_2, \Delta_3, \Delta_4 > 0$.

It will also prove useful to fit this condition by defining the degree of instability (DOI) of the system as follows:

$$\mathrm{DOI}(\mathbf{A}) = \mathrm{Max}(\mathrm{Re}(\mathrm{Eig}(\mathbf{A}))) \tag{2.59}$$

Whenever this number is positive, it means at least one of the Hurwitz coefficients is zero and the system is unstable. When $\mathrm{DOI}(\mathbf{A}) < 0$, the system is stable. The case when the degree of instability equals zero will not be treated as this case has measure zero in the corresponding probability space.

3 Case Study

The methodology developed to assess yaw stability in a 3-DOF framework will now be applied to the specific case of an ongoing EU Horizon project called Oceanbird. The concept, as it is being developed by Wallenius Wilhelmsen and Alfa Laval, in collaboration with multiple partners in the wind propulsion industry, aims to develop oceangoing RoRo vessels able to transport several thousands of cars across the Atlantic Ocean, using wind as the main means of propulsion. An artistic rendition is shown in Figure 3.1.

In the context of the Oceanbird project, two demonstrator vessels are currently being built. The first vessel, named Tirranna, is a retrofit that is currently in the process of equipping one wingsail on its deck. Full-scale trial data from Tirranna serves as a testbed for the next generation of vessels - in particular, the second demonstrator vessel, named Orcelle Wind. This will be a new build with multiple wingsails, using wind as the main source of propulsion. The latest design iteration has six wingsails, a length of $206.6\,\mathrm{m}$, a beam of $39\,\mathrm{m}$ and a height of $70\,\mathrm{m}$ above water, boasts a capacity of 7100 car units and is expected to emit at least $50-60\%$ less than conventional car carriers [22].

For the case study, a design iteration of the Oceanbird concept will be used for which there was sufficient data readily available. The main design constants, as well as the aerodynamic and hydrodynamic parameters, were provided by RISE SSPA (`https://www.ri.se/en/what-we-do/maritime`).

Quantity Name	Symbol	Quantity
Length	L	$206.6\,\mathrm{m}$
Beam	B	$39\,\mathrm{m}$
Draft	T	$8.5\,\mathrm{m}$
Displacement	∇	$30\,843\,\mathrm{m}^3$
Longitudinal CoM position	x_g	$-9.8\,\mathrm{m}$
Yaw radius of gyration	k_{zz}	$72.1\,\mathrm{m}$

Table 3.1: Main vessel data of the wPCC

The wPCC has four wingsails placed at the centreline of the vessel, where the mean centre of effort approximately crosses the axis of rotation so as to not cause difficulties with regards to control of the angle of attack. In Table 3.2, the main aerodynamic data of the ship is given, as well as the air density and the reference area used for calculating the wind force exerted on the superstructure. The shape of the sail is given by discrete values for the chord lengths at 25 different sections of the sail. Table 3.3 presents the exact chord lengths at 25 linearly spaced chords along the height of the sail. The wingsails have a NACA 0015 profile, which is a symmetrical shape. This has the advantage of being able to generate lift on both starboard and port wind directions without deforming. Figure 3.2 shows the measured drag and lift coefficients against the angle of attack. To be able to calculate aerodynamic

Figure 3.1: Orcelle car carrier developed by Oceanbird

Quantity Name	Symbol	Quantity
Air density	ρ_a	$1.225\,\mathrm{kg\,m^{-3}}$
Reference area for wind forces	A_T	$1229\,\mathrm{m}^2$
Sail area	A_S	$7376\,\mathrm{m}^2$
Sail height	h_S	$80\,\mathrm{m}$
Sail foot above water line	h_B	$27\,\mathrm{m}$
Longitudinal CoE of sail 1	$x_{S,1}$	$-61.6\,\mathrm{m}$
Longitudinal CoE of sail 2	$x_{S,2}$	$-18.4\,\mathrm{m}$
Longitudinal CoE of sail 3	$x_{S,3}$	$24.8\,\mathrm{m}$
Longitudinal CoE of sail 4	$x_{S,4}$	$68.0\,\mathrm{m}$

Table 3.2: Aerodynamic constants and parameters

Height above h_B (m)	l_C (m)	Height above h_B (m)	l_C (m)	Height above h_B (m)	l_C (m)
1.6	26.5663	30.4	25.3884	59.2	20.9925
4.8	26.5544	33.6	25.1076	62.4	20.0252
8.0	26.5124	36.8	24.7945	65.6	18.9216
11.2	26.4403	40.0	24.4482	68.8	17.6874
14.4	26.3385	43.2	24.0647	72.0	16.3276
17.6	26.2072	46.4	23.6286	75.2	14.8471
20.8	26.0467	49.6	23.1215	78.4	13.25
24.0	25.8571	52.8	22.5251		
27.2	25.638	56.0	21.8213		

Table 3.3: Discrete chord lengths of the wingsail

forces for any angle of attack, an interpolation function is needed. Since the stability evaluation method described in the methodology section uses force derivatives of first degree, the interpolation function is required to be continuously differentiable in order to avoid discontinuities in the stability evaluation. Therefore, a spline method of order 2 was used to ensure that the interpolation function is continuously differentiable. The aerodynamic profile for negative angles of attack was consequently extrapolated according to $C_D(-\alpha) = C_D(\alpha)$ and $C_L(-\alpha) = -C_L(\alpha)$. This follows by symmetry of the airfoil.

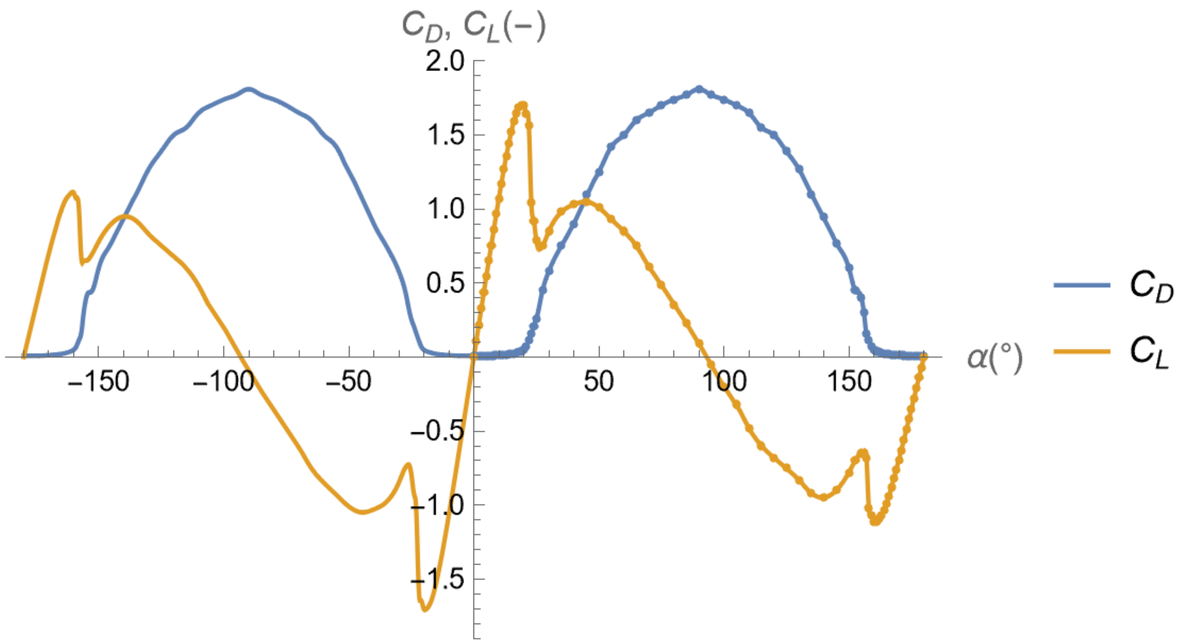

Figure 3.2: Measured aerodynamic coefficients for NACA 0015 airfoil, including 2-degree interpolation spline

Since the interaction effects between the four sails are expected to be both less predictable and larger in magnitude when entering angles of attack beyond the stall angle $(|\alpha| > 20°)$, the sails are constrained to always stay within the no-stall region. This practice allows for a relatively simple polynomial approximation of the drag and lift coefficients. It turns out that for a NACA 0015 airfoil such as used in the example case, the drag and lift coefficients in the non-stall region can be approximated really well by the following polynomials obtained by a least-square fit on even (drag) resp. uneven (lift) polynomials of degree at most 5:

$$\begin{bmatrix} C_D(\alpha) \\ C_L(\alpha) \end{bmatrix} = \begin{bmatrix} 0.008163 + 0.03283\alpha^2 + 2.286\alpha^4 \\ 6.196\alpha + 1.127\alpha^3 - 97.70\alpha^5 \end{bmatrix} \tag{3.1}$$

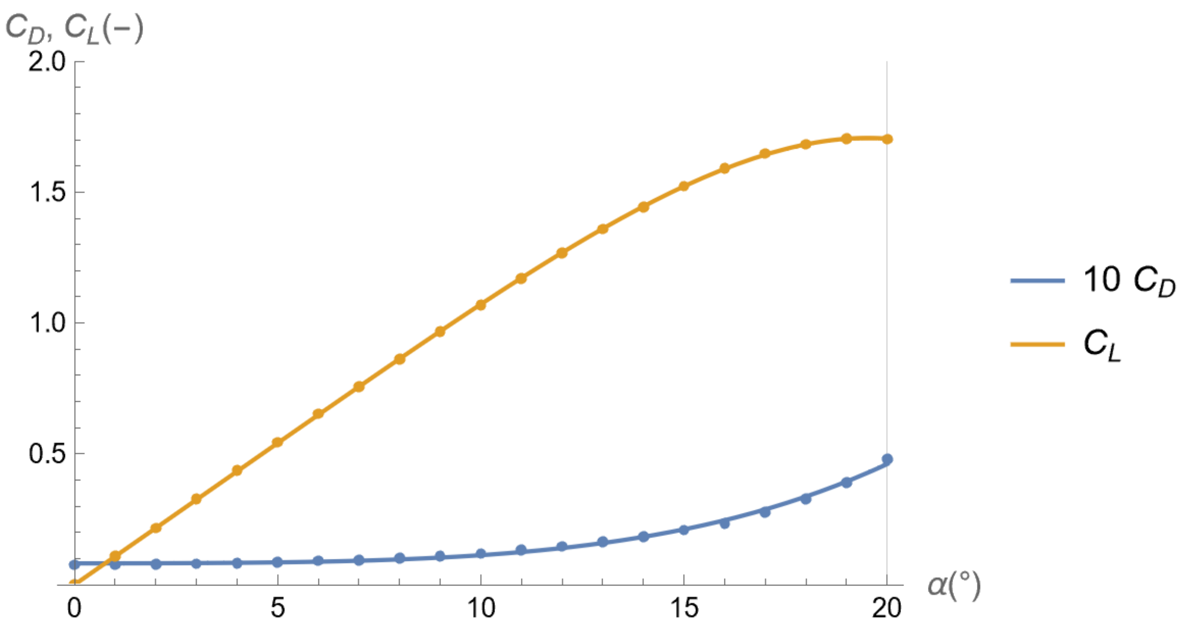

Figure 3.3: Measured aerodynamic coefficients for NACA 0015 airfoil in no-stall region, including interpolation polynomial

Using polynomial approximations for the aerodynamic coefficients means simple expressions exist for both the functions and their derivatives over the whole domain. The polynomial fits are shown in Figure 3.3.

In the used model, the aerodynamic forces on the hull depend on the apparent wind angle at the origin. The measured data follows from virtual tests and correspond closely to data found in the literature for similar hull shapes. Again, an interpolation spline of degree 2 was used in combination with symmetry laws in order to cover all possible values of the apparent wind angle θ_A. The result is shown in Figure 3.4.

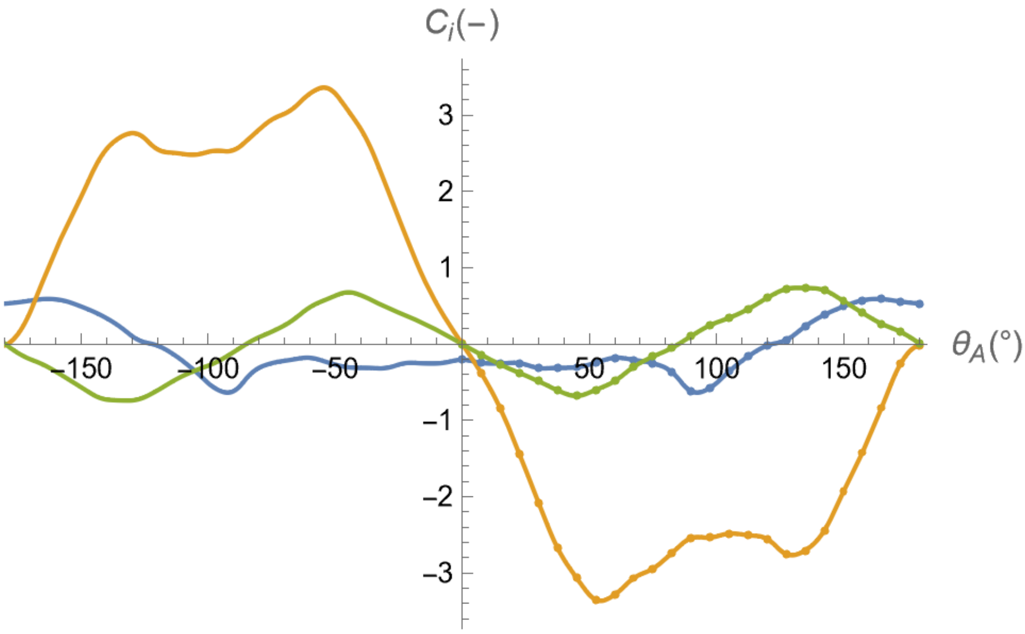

Figure 3.4: Measured aerodynamic coefficients of the superstructure depending on apparent wind angle, including 2-degree interpolation spline

In order to obtain the hydrodynamic coefficients, the model was subjected to a so-called Virtual Captive Test (VCT), which means that a high-fidelity flow model was used on a virtual hull to perform the same kind of trials that would be used in a towing tank to fit a polynomial manoeuvring model to a scale model of a vessel. Two fitting models were used: one that is linear in sway and yaw, and a more nonlinear model having nonzero coupling forces in sway and yaw. For brevity, they will be referred to as the linear resp. nonlinear model.

Figure 3.5 and 3.6 clearly illustrate the difference between the two manoeuvring models that were used. Both the data and the zigzag test in the figures are due to Martin Alexandersson at RISE SSPA. The exact coefficients are shown in Table 3.4 and 3.5.

Quantity	Value	Quantity	Value	Quantity	Value
X'_0	-0.00121944	Y'_v	-0.012095	N'_v	-0.00122871
X'_u	0.000616273	Y'_r	0.0	N'_r	-0.00219559
X'_{vv}	0.000980115	Y'_{vvv}	0.0	N'_{vvv}	0.0
X'_{vr}	0.000423671	Y'_{vvr}	0.0	N'_{vvr}	0.0
X'_{rr}	0.000144873	Y'_{vrr}	0.0	N'_{vrr}	0.0
$X'_{\delta\delta}$	-0.00302748	Y'_{rrr}	0.0	N'_{rrr}	0.0
		Y'_δ	0.00459817	N'_δ	-0.0022101
		$Y'_{\delta\delta\delta}$	0.00673454	$N'_{\delta\delta\delta}$	-0.00338169
		$Y'_{r\delta\delta}$	0.0	$N'_{r\delta\delta}$	0.0
		$Y'_{rr\delta}$	0.0	$N'_{rr\delta}$	0.0
		$Y'_{v\delta\delta}$	0.0	$N'_{v\delta\delta}$	0.0
		$Y'_{vv\delta}$	0.0	$N'_{vv\delta}$	0.0
		$Y'_{vr\delta}$	0.0	$N'_{vr\delta}$	0.0

Table 3.4: Hydrodynamic coefficients for linear model fitted to VCT data

Quantity	Value	Quantity	Value	Quantity	Value
X'_0	-0.00121944	Y'_v	-0.0104463	N'_v	-0.000961098
X'_u	0.000616273	Y'_r	0.00370091	N'_r	-0.00198337
X'_{vv}	0.00203195	Y'_{vvv}	-0.0593839	N'_{vvv}	-0.0107814
X'_{vr}	0.00104735	Y'_{vvr}	-0.0649034	N'_{vvr}	-0.0391047
X'_{rr}	-0.000264788	Y'_{vrr}	-0.0437891	N'_{vrr}	-0.00566021
$X'_{\delta\delta}$	-0.00302748	Y'_{rrr}	-0.00385248	N'_{rrr}	-0.00262059
		Y'_δ	0.00459817	N'_δ	-0.0022101
		$Y'_{\delta\delta\delta}$	0.00673454	$N'_{\delta\delta\delta}$	-0.00338169
		$Y'_{r\delta\delta}$	0.0	$N'_{r\delta\delta}$	0.0
		$Y'_{rr\delta}$	0.0	$N'_{rr\delta}$	0.0
		$Y'_{v\delta\delta}$	0.0	$N'_{v\delta\delta}$	0.0
		$Y'_{vv\delta}$	0.0	$N'_{vv\delta}$	0.0
		$Y'_{vr\delta}$	0.0	$N'_{vr\delta}$	0.0

Table 3.5: Hydrodynamic coefficients for nonlinear model fitted to VCT data

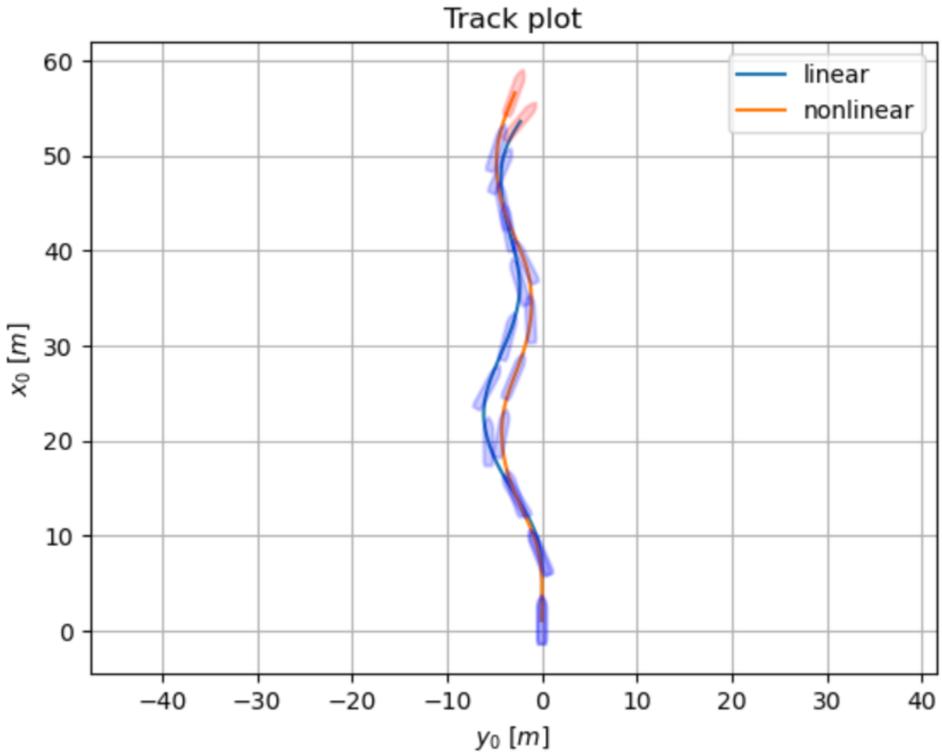

Figure 3.5: Manoeuvring model zigzag test comparison - spatial plot

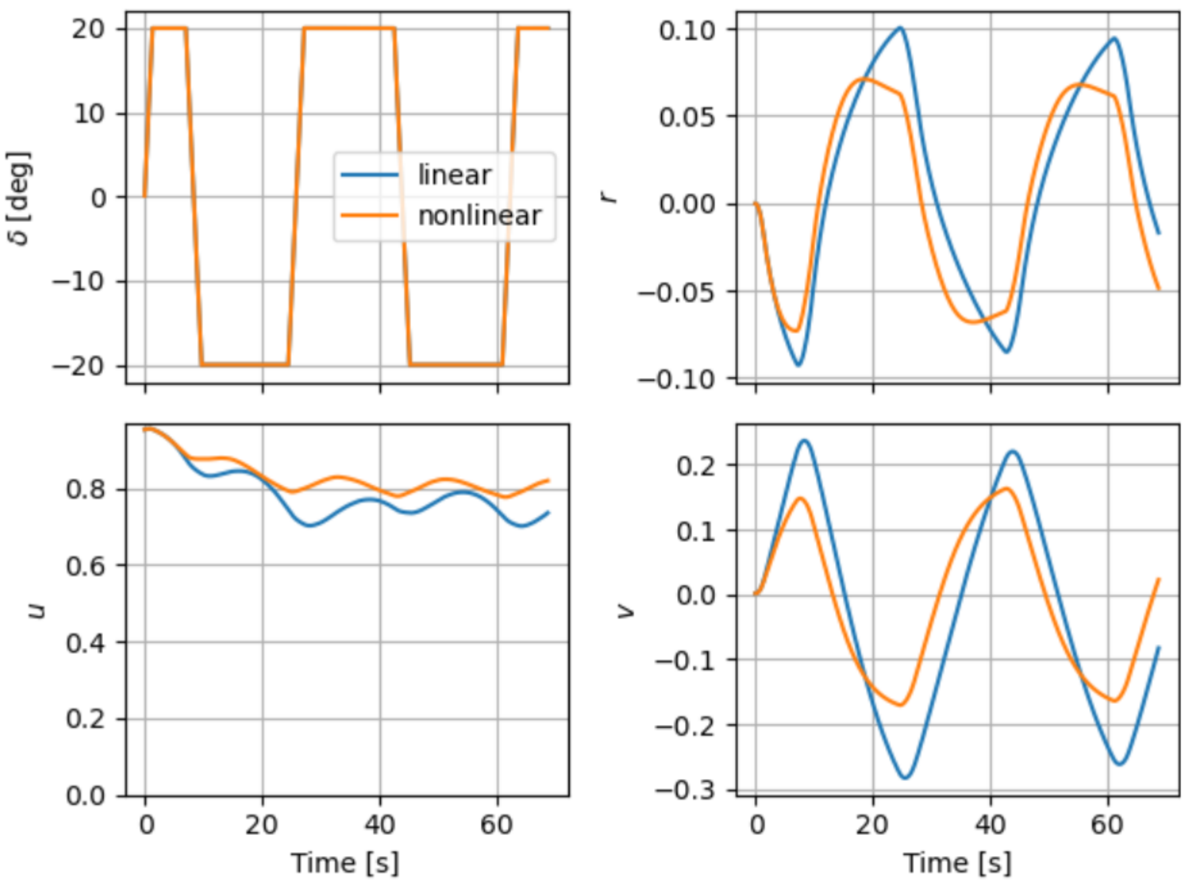

Figure 3.6: Manoeuvring model zigzag test comparison - rudder angle and velocities

4
Results

4.1. Steady state results

All of the results have been obtained by implementing the described model in Wolfram Mathematica. The script used to obtain the data can be requested by contacting guidohaenen@gmail.com, while intermediate VPP results have been presented here in Appendix A.

The constrained optimisation algorithm was first run with four different underlying hydrodynamic models, using the relatively simple uniform flow model. Both of the models given in Table 3.4 and 3.5 result in stable hulls in terms of the classical stability criterion $Y'_v(N'_r - m'x'_g) + (m' - Y'_r)N'_v > 0$, which is the binary diagnostic of stability at zero drift without considering aerodynamics. As an attempt to verify the methodology of evaluating the sign of the maximum of the real part of the eigenvalues of the system transition matrix, the method should produce unstable results for a hull that is inherently more unstable in the classical sense. Therefore, both models were used as well as their tweaked "unstable" counterparts. In the modified models, the original coefficients N'_v and N'_r were respectively multiplied by 2 and divided by 3.

The steady-state data resulting from the algorithm consists of steady velocities u_0 and v_0, as well as a steady rudder angle δ_0 and steady sheeting angles $s_{1,0}, \ldots, s_{4,0}$.

The results, showing the resulting ship speed $U = \sqrt{u_0^2 + v_0^2}$ for every true wind angle TWA (see below for the definition of TWA) are shown in Figure 4.1. A wind speed of $8\,\mathrm{ms}^{-1}$ was used, which is weak enough that in a 4-DOF model, the heeling constraints would be satisfied even without having to reef the sails [15]. True wind angles θ_W varied between $32°$ and $160°$. It is clear that the model differences do not have a large effect on the outcome of the VPP algorithm. This observation, along with the general magnitude of the numbers found, strengthens confidence in the validity of the method.

A transformation $\theta_w \mapsto \theta_w - \beta_0 =: TWA$ was made so that the angles shown in the plot refer to true wind angles with respect to the speed over ground (SOG), which is the standard practice for VPP results. The fact that the drift angle as a function of the true wind is a bijection means that this can be done without loss of information. The reason for defining θ_w with respect to the bow was to align with the previous work on yaw stability in steady wind [25]. The reason for using TWA in the VPP plot is just a presentation convention that allows for comparison with other VPP plots and has no effect on the stability assessment. The steady-state ship velocities resulting from the SEAMAN VPP used by RISE/SSPA and applied to the stable ship hull is included in Figure 4.1. It can be observed that the results are very close. The force model developed in this thesis thus produces credible results, at least for the steady state calculation.

4.2. Open-loop stability assessment

For all four hydrodynamic models, the steady state data served to calculate the numerical value of the $\mathbf{A}$ and $\mathbf{B}$ matrices. This allowed for a direct computation of the eigenvalues of the $\mathbf{A}$ matrix for every

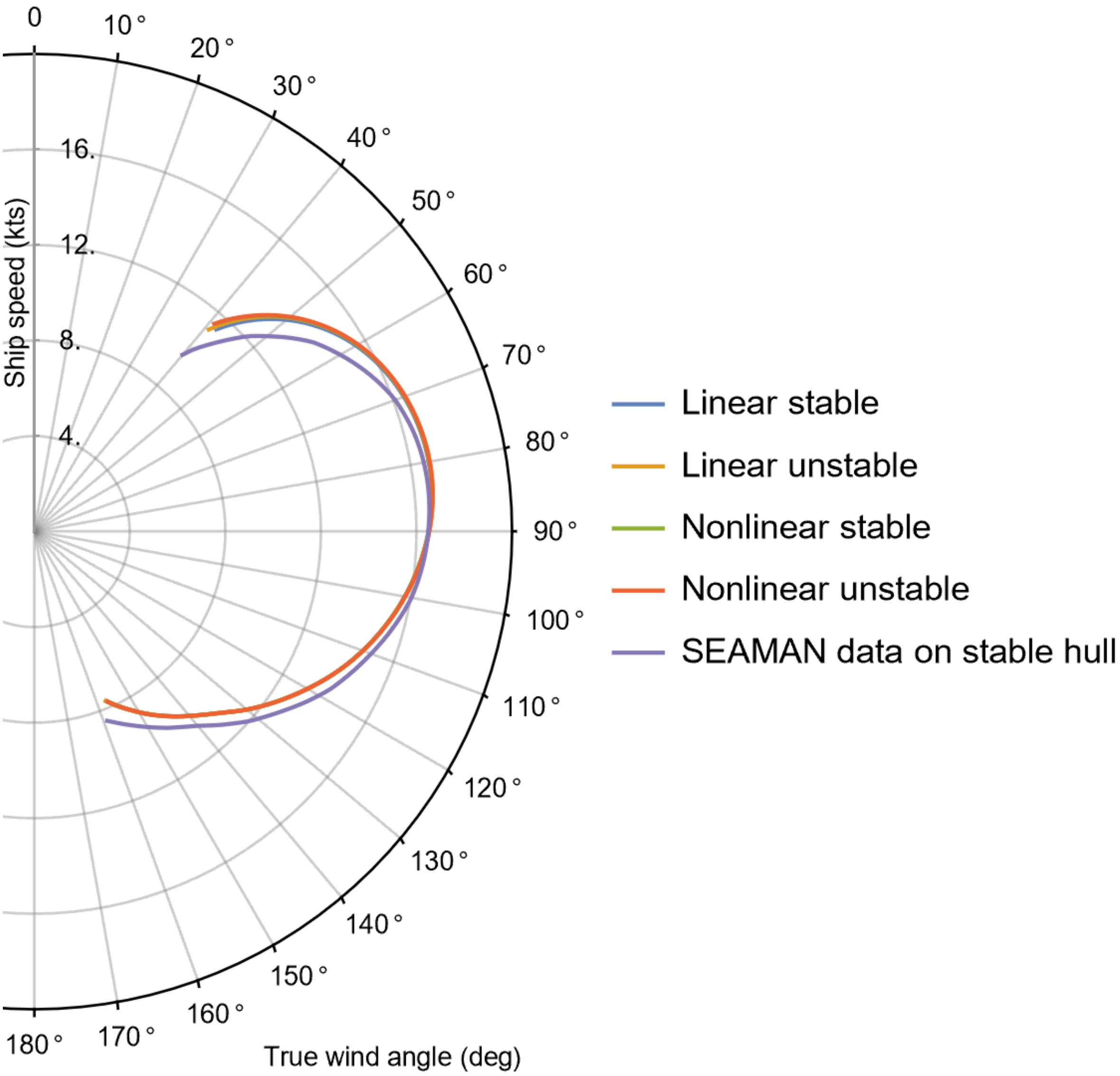

Figure 4.1: VPP results for four different hydrodynamic models, $V_{10m} = 8\,\mathrm{ms}^{-1}$

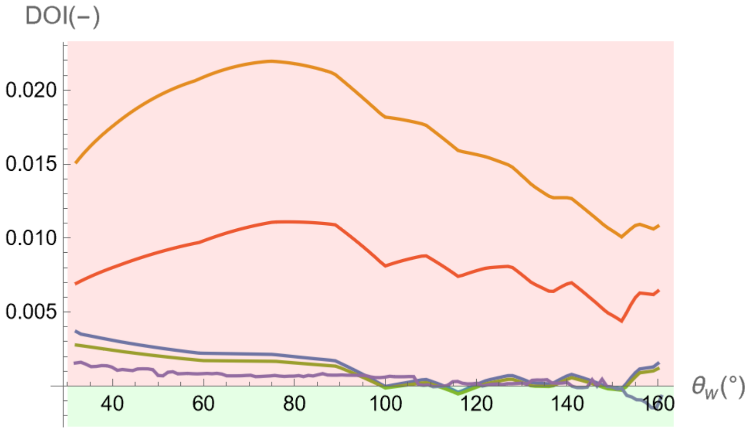

Figure 4.2: Open-loop degree of instability for four different hydrodynamic models, $V_{10m} = 8\,\mathrm{ms}^{-1}$

θ_W, of which the real parts were then calculated. The largest value served as a marker for whether the open-loop system was stable. This is also called the "degree of instability" or DOI, which was earlier defined in Equation 2.59. To verify that all derivations were correctly implemented, the found DOI values were verified by running a simple Euler scheme on a few steady states of both stability types. The results are presented in Figure 4.2, where the stable and unstable regions are shaded green and red, respectively. Any subsequent stability plot will follow the same convention. An almost stepwise linear behaviour can be discerned when looking at Figure 4.2. This cannot result from a small data resolution, since a step size of $1°$ was used when varying θ_W, and the steps in the graph have a larger step size. Future studies could delve into the exact mechanisms at play here by unpacking the Hurwitz coefficients and exploring how they evolve under a varying true wind angle.

Furthermore, it is rather surprising that for the "stable hull" cases, there exist several disconnected intervals of θ_W values that yield a stable steady equilibrium. This means that for those wind angles, the helmsman could fix the rudder position and the sheets and go on a coffee break without the ship veering out of control - all while using sail propulsion and sailing under a drift angle. For most wind angles, however, the ship cannot maintain a stable heading without any form of active steering. This is in line with the general intuition that one could have in the context of sailing vessels. The few stability islands mentioned above might even disappear when a 4-DOF model or a more accurate aerodynamic interaction model would be used instead of the basic approximation of the current methodology.

A more obvious observation that one would hope to see is the fact that artificially destabilised hulls do in fact yield more unstable eigenvalues when operating in full sailing mode. This further solidifies the validity of the results.

An attempt was made in the methodology section to derive a general analytical criterion. Due to the exponentially increasing complexity of the Routh-Hurwitz criterion with each new added dimension, the expressions were rather cumbersome and unwieldy. For actual applications, the system matrices could be calculated just as well by perturbing all the forces described around the steady state with small values ε, thus obtaining all the necessary partial derivatives to fill in the force derivatives. This has its own drawbacks, seeing as it would require five times as many force evaluations - one for the steady state solution and one for each dimension of the state vector. Applications of the Hurwitz method could prove superior in cases where computational time required for the force calculations is longer than the time required to fill in the force matrix from the steady state information alone.

In this specific case, it turns out that for all the wind angles analysed $\theta_w \in [32°, 160°]$, the Hurwitz coefficients $\Delta_1, \ldots, \Delta_3 > 0$ and it is purely the coefficient Δ_4 that determines open-loop yaw stability. In Figure 4.3, this is visualised. It can be seen that the sign of the DOI quantity is larger than zero if and only if the quantity $\Delta_4' := \frac{\Delta_4}{\frac{1}{8}\rho^3 L^7 V_{10m}^4}$, a nondimensional version of Δ_4, is smaller than zero. It would be very interesting to see whether this reduction of the Routh-Hurwitz conditions is possible in a more general marine engineering context, or if it is exclusive to the particular hull and force model being used.

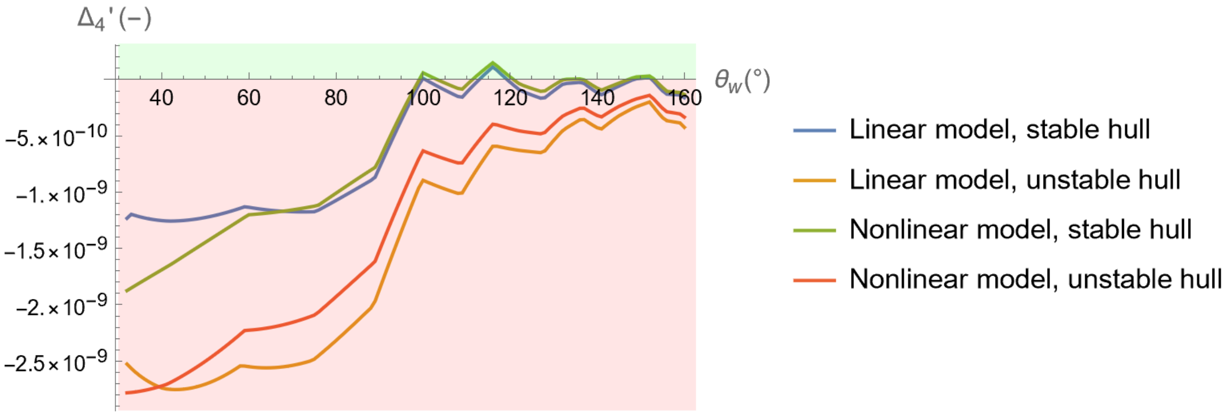

Figure 4.3: Fourth Hurwitz coefficient at various true wind angles.

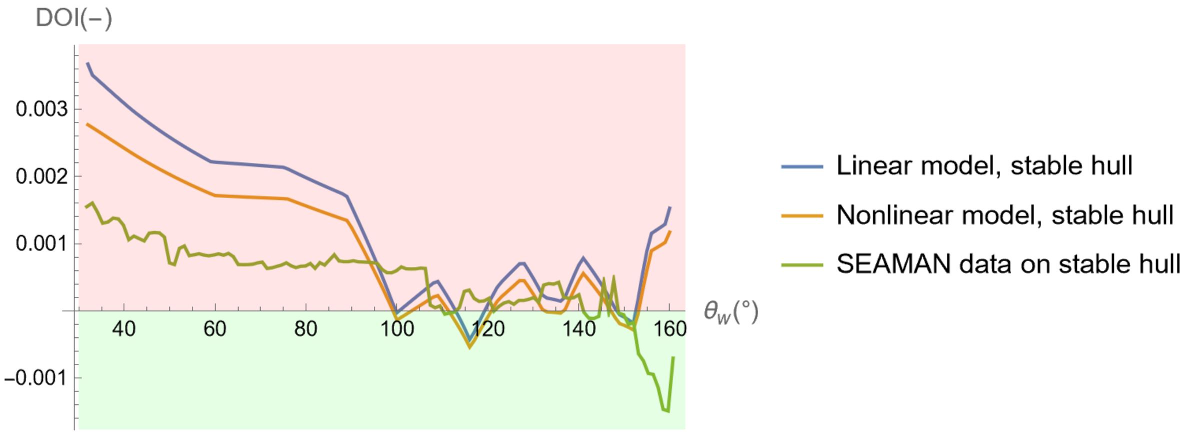

Figure 4.4: Open-loop degree of instability for both analytical models compared with SEAMAN results

In the former case, the stability criterion would look as follows:

$$X_{t,\psi}Y_{t,v}N_{t,u} + X_{t,u}Y_{t,\psi}N_{t,v} + X_{t,v}Y_{t,u}N_{t,\psi} > X_{t,v}Y_{t,\psi}N_{t,u} + X_{t,\psi}Y_{t,u}N_{t,v} + X_{t,u}Y_{t,v}N_{t,\psi} \tag{4.1}$$

A sanity check for whether the found DOI values are reasonable, can be done by comparing them with the values obtained by discrete differentiation of the SEAMAN VPP used by RISE SSPA as it was applied on the stable hull case. In this case, for every steady state resulting from the optimisation problem, a very small perturbation was made in the direction of every state variable, which yielded corresponding matrices $\mathbf{A}$ and $\mathbf{B}$ for the chosen operational conditions. Essentially, the force matrices were filled in by taking difference quotients of the forces as calculated by the SEAMAN algorithm. The resulting matrices are due to data delivered by Fredrik Olsson at RISE SSPA. This data yielded numerically estimated system matrices $\mathbf{A}$ of which the DOI value was plotted in Figure 4.4 together with the data resulting from the model in this thesis. It can be concluded that the analytical stability assessment is indeed reasonable as it roughly agrees with the SEAMAN-produced data - both concerning order of magnitude of the DOI and concerning its general trend when comparing different points of sail.

The results found by the method developed in the methodology section agree quite well with the SEAMAN data. Both methods show open-loop instability at the upwind points of sail and marginal stability on a beam reach. The results slightly diverge again as the wind angle approaches $160°$, which may be explained by interaction effects (not modelled in the methodology but present in SEAMAN data) which become stronger when the sails block each other more.

4.3. Modelling approaches

In order to gain a more in-depth understanding of the modelling limits of the applied methodology, two additional variations were made in the open-loop stability assessment.

4.3.1. Wind flow model

The first variation pertains to the wind strength variations over the height. Both a model with an atmospheric boundary layer and one without a boundary layer but with a constant wind profile over the height (multiplying V_{10m} by a correction factor of 1.285 to adjust for the average forces on the sail in the boundary layer model) were used. The results (using only the linear hydrodynamic model for a stable hull) are shown in Figure 4.5, using the same conventions as in Figure 4.1. Again, the steady-state

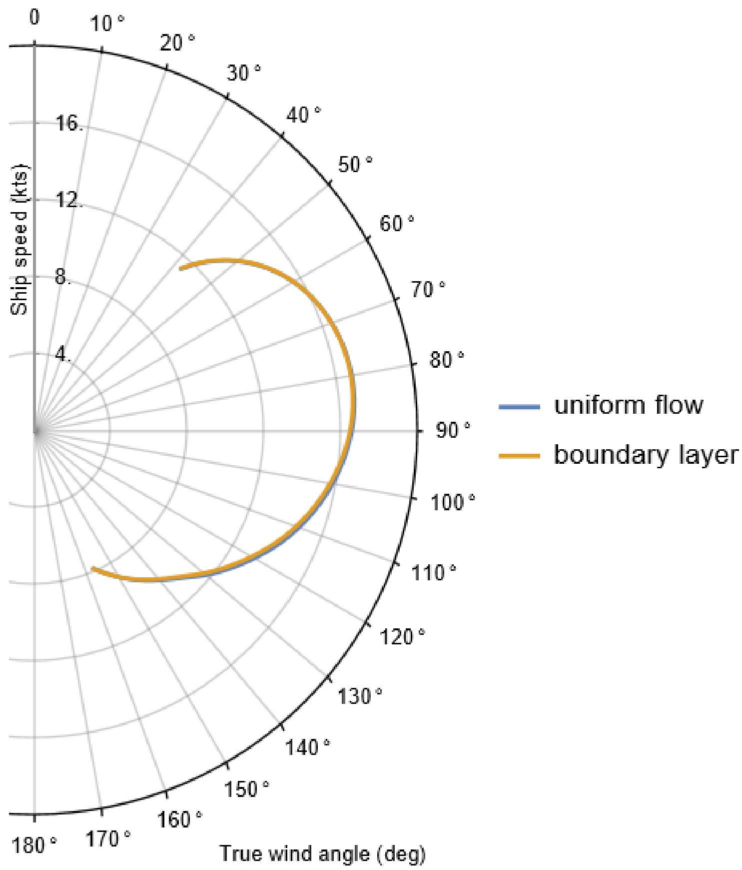

Figure 4.5: Ship speed from VPP at $V_{10m} = 8\,\mathrm{ms}^{-1}$ for uniform-flow model and boundary layer model, using linear stable hull.

differences between both models are virtually equal. This is a priori not a guarantee that the force derivatives also behave the same. Nonetheless, they actually do behave roughly the same, as can be seen by the DOI plot in Figure 4.6. From the above results, it can be concluded that the application of a model with an atmospheric boundary layer does not lead to substantial qualitative stability differences when compared with the uniform flow model that uses a wind speed correction factor. The difference in computational effort is huge, therefore an important takeaway is that the exact distribution of the wind profile and resulting twist effects are of negligible importance when assessing directional stability.

4.3.2. Surge coupling

Since this thesis builds on the previous work done on the yaw stability of a ship in steady wind by adding sails to the equation, it makes sense to gauge the effect of surge coupling on stability as the thrust-yaw coupling on force is expected to be considerably larger than for propeller-driven vessels. The state

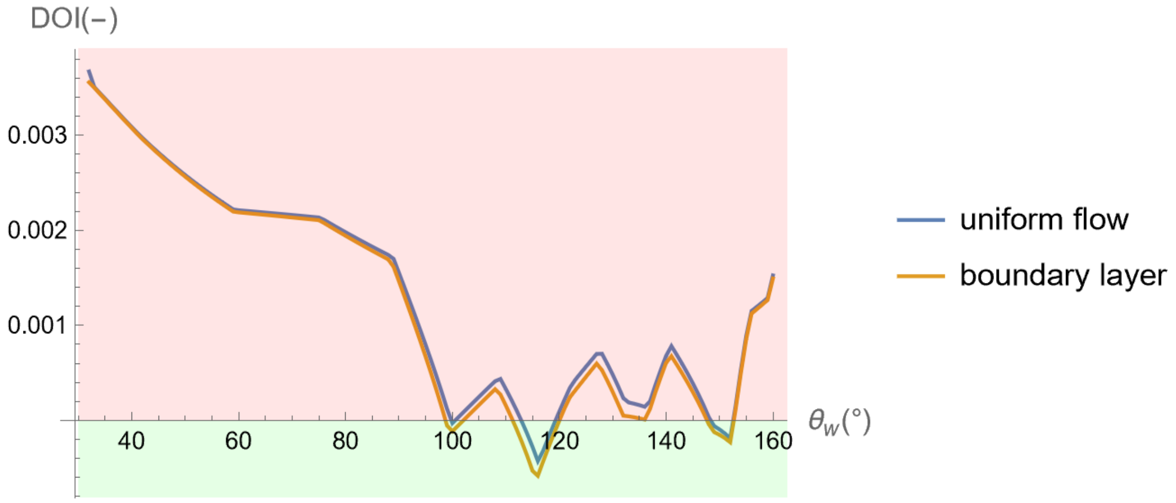

Figure 4.6: Degree of instability for two different flow models, using the linear stable hull type.

transition matrix $\mathbf{A}$ is first explicitly written out in symbolic coefficients:

$$\mathbf{A} = \begin{bmatrix} a_{11} & a_{12} & a_{13} & a_{14} \\ a_{21} & a_{22} & a_{23} & a_{24} \\ a_{31} & a_{32} & a_{33} & a_{34} \\ 0 & 0 & 1 & 0 \end{bmatrix} \tag{4.2}$$

An attempt to simplify this system can be made by defining the no-surge state transition matrix, which is the bottom-right part of the original state transition matrix:

$$\mathbf{A}_{NS} := \begin{bmatrix} a_{22} & a_{23} & a_{24} \\ a_{32} & a_{33} & a_{34} \\ 0 & 1 & 0 \end{bmatrix} \tag{4.3}$$

The Hurwitz criterion can be formulated again from the no-surge state transition matrix $\mathbf{A}_{NS}$. Again, all Hurwitz coefficients turn out positive except for the last one, which determines the overall stability of the sway-yaw system. This corresponds to the D_4 quantity from [25] and is reformulated here using the notation applied to the no-surge (subscript NS) case:

$$\Delta_{3,NS} = Y_{t,v}N_{t,\psi} - Y_{t,\psi}N_{t,v} \tag{4.4}$$

Whenever this quantity is larger than zero, the course will be stable for this particular vessel. For other vessels, the other Hurwitz coefficients may further restrict the stability of the system.

The degree of instability for the restricted matrix was plotted in Figure 4.7 for all steady-state results, and a comparison can be made with the original surge-coupled case. The results are similar, although stable equilibria become unstable in some beam reach points of sail after neglecting the surge coupling. Another main observation is the divergence of the results in headwinds. Although the stability type remains unstable in the whole region $\theta_w \in [32°, 80°]$, the surge coupling could be expected to yield qualitative differences with regards to stability in another situation - for example, when considering a different vessel or when adding the influence of rudder feedback.

Unlike in the case of the atmospheric boundary layer, in this case the results are too different to be able to neglect surge couplings.

4.4. Closed-loop analysis

To add the influence of rudder feedback on yaw motion, a K matrix is defined according to a proportional/derivative (PD) control scheme. Note the gain values are multiplied by -1 to account for the sign

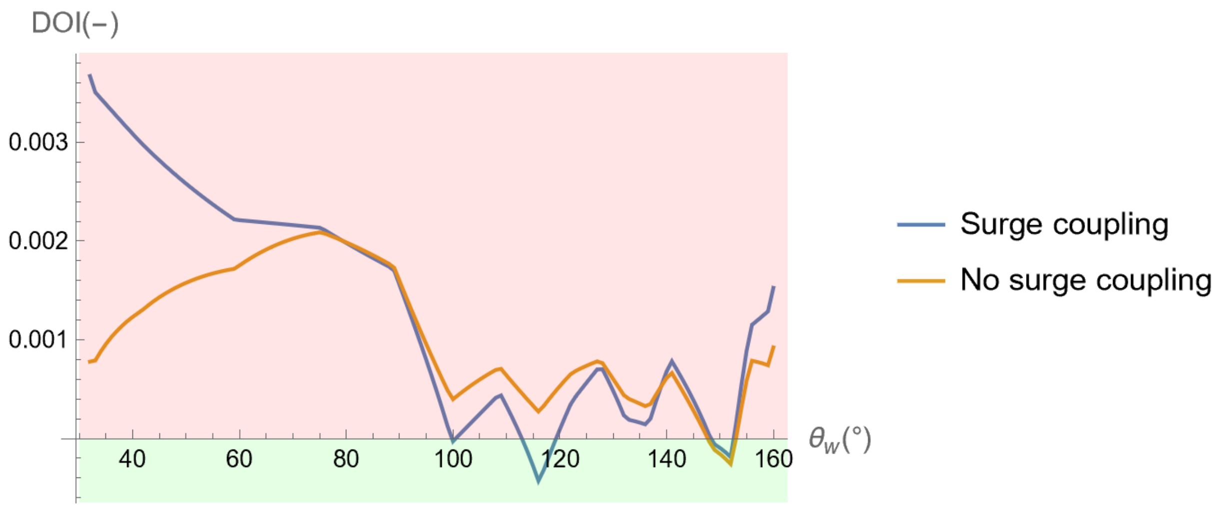

Figure 4.7: Degree of instability of the vessel system both with and without surge coupling, using the linear stable hull type.

convention of δ combined with the usual notation of feedback, that is, $\mathbf{A}-\mathbf{BK}$.

$$\mathbf{K}(G_1, G_2) := \begin{bmatrix} 0 & 0 & -G_2 & -G_1 \\ 0 & 0 & 0 & 0 \\ 0 & 0 & 0 & 0 \\ 0 & 0 & 0 & 0 \\ 0 & 0 & 0 & 0 \end{bmatrix} \tag{4.5}$$

A simple first implementation is a control scheme with only a proportional gain of $G_1 = 0.3$ ($G_2 = 0$), representing human steering:

$$\mathbf{K}_{human} := \begin{bmatrix} 0 & 0 & 0 & -0.3 \\ 0 & 0 & 0 & 0 \\ 0 & 0 & 0 & 0 \\ 0 & 0 & 0 & 0 \\ 0 & 0 & 0 & 0 \end{bmatrix} \tag{4.6}$$

A control scheme which is expected to be more powerful is given by proportional and derivative gains $G_1 = G_2 = 1.0$, which more closely resembles how an autopilot would steer the vessel.

$$\mathbf{K}_{auto} := \begin{bmatrix} 0 & 0 & -1.0 & -1.0 \\ 0 & 0 & 0 & 0 \\ 0 & 0 & 0 & 0 \\ 0 & 0 & 0 & 0 \\ 0 & 0 & 0 & 0 \end{bmatrix} \tag{4.7}$$

The closed-loop DOI is then calculated again by taking the maximum of the real parts of the eigenvalues of the system matrix, which in this case is equal to $\mathbf{A}-\mathbf{BK}$ rather than just $\mathbf{A}$ like it was in the open-loop case. The result is seen in Figures 4.8 and 4.9, where a comparison was again made between four different sets of hydrodynamic coefficients as described in the beginning of the Results section. The vessel is now steerable at all the analysed points of sail, as is to be expected since it was originally designed to be wind-propelled. The nonlinear model of the same hull gives virtually the same results as the linear model. The tweaked destabilised hulls have closed-loop eigenvalues further to the right (as seen in the complex plane) which makes them more unstable in the wind-propelled context, as expected. The destabilised hull resulting from the nonlinear hydrodynamic model is less affected than the one that came from a linear model, which can be expected since the linear terms are also the ones that were tweaked and in a nonlinear model, overall stability under a drift angle depends not only on the linear coefficients that appear in the classical stability criterion. The autopilot control case, like the human control case, showcases a drastically improved stability under all points of sail when compared to the open-loop case. There is less added effect of PD control when using the original hull, while

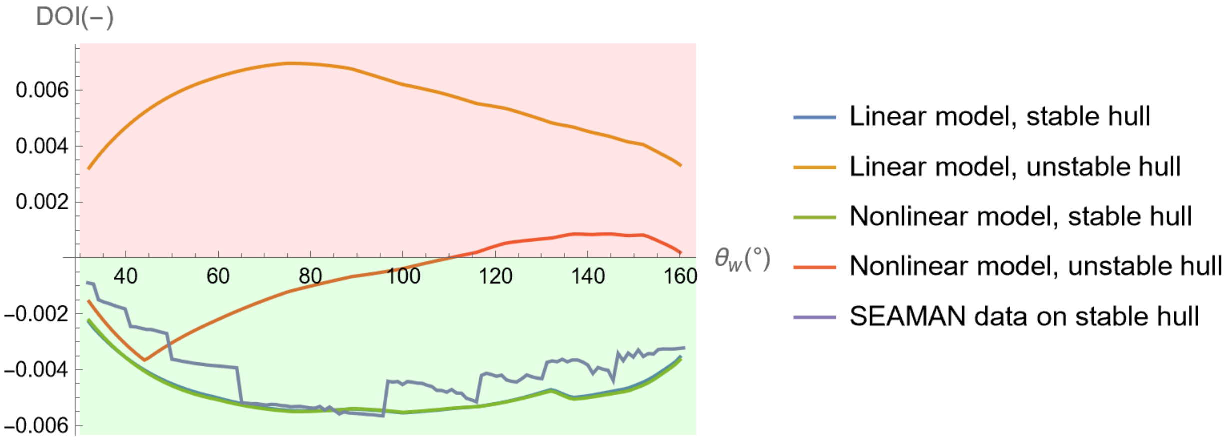

Figure 4.8: Closed-loop degree of instability of human steering control ($G_1 = 0.3, G_2 = 0$).

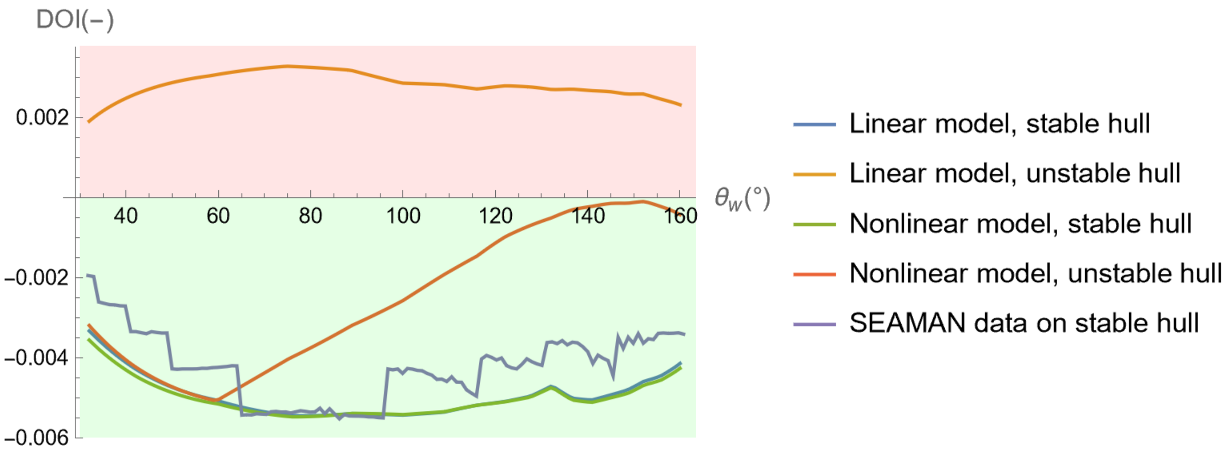

Figure 4.9: Closed-loop degree of instability of automatic steering control ($G_1 = 1.0, G_2 = 1.0$).

the tweaked hulls benefit a little from the effect of adding derivative control. The DOI of the nonlinear unstable model closely follows its stable counterparts for closed-hauled points of sail, and then starts increasing after what is likely a bifurcation in the eigenvalue space (note that taking the maximum of the real parts of the eigenvalues means that at certain points, when changing the underlying parameters, the eigenvalues can flip positions, which is likely to have happened here).

The plots in Figures 4.8 and 4.9 again include the numerically obtained data from the SEAMAN software used by RISE SSPA, applied on the stable hull type. The data agrees quite well with the results obtained from the analytical method.

The unstable hulls used in this thesis are more hypothetical and only result from artificially tweaking the hydrodynamic coefficients. An interesting direction of further research would be to investigate these same characteristics for a refit of a real unstable vessel (or at the very least a parameter set that was directly derived from VCT data), e.g. a tanker or bulk carrier.

4.5. Yaw motion

For the last research question, the time-domain behaviour of the closed-loop system is examined to get an idea of the robustness of the step response. Also, the general method of solving the associated ODE with boundary conditions is presented.

The yaw motion can be calculated starting from an equilibrium operational point and subsequently assuming a new target yaw angle ψ_r in order to simulate a step response. Recall Equation 2.52 and assume constant sheeting angles to investigate the ship/rudder system around a constant equilibrium point:

$$\begin{bmatrix} \dot{u} \\ \dot{v} \\ \dot{r} \\ \dot{\psi} \end{bmatrix} = \overbrace{\left[\begin{array}{cccc} & \mathbf{M}^{-1} \cdot \mathrm{D}_{\mathbf{x}}\mathbf{F}_{tot} & & \\ \hline 0 & 0 & 1 & 0 \end{array}\right]}^{\mathbf{A}} \begin{bmatrix} \Delta u \\ \Delta v \\ r \\ \psi \end{bmatrix} + \overbrace{\left[\begin{array}{c} \mathbf{M}^{-1} \cdot \mathrm{D}_{\mathbf{u}}\mathbf{F}_{tot} \\ \hline \mathbf{0} \end{array}\right]}^{\mathbf{B}} \begin{bmatrix} \Delta\delta \\ 0 \\ \vdots \\ 0 \end{bmatrix} \tag{4.8}$$

When rewriting the ODE system of Equation 4.8 so that u and v are eliminated, a fourth-order differential equation is the result:

$$a_0 \dddot{r} + a_1 \ddot{r} + a_2 \dot{r} + a_3 r + a_4 \psi = q_1 \ddot{\delta} + q_2 \dot{\delta} + q_3 \Delta\delta \tag{4.9}$$

Here the a_i coefficients are the same as in Equation 2.53, while the q_i coefficients are found by unpacking the definitions of $\mathrm{D}_{\mathbf{u}}$ and the mass matrix $\mathbf{M}$. As before, the entire equation was first multiplied by $\det(\mathbf{M})$ in order to clear out the bulky fractions resulting from inverting the mass matrix. After unpacking everything, the q_i coefficients are as follows:

$$\begin{aligned} q_1 &= m_{11}m_{22}N_{t,\delta} - m_{11}m_{32}Y_{t,\delta}; \\ q_2 &= m_{11}Y_{t,\delta}N_{t,v} - m_{11}Y_{t,v}N_{t,\delta} + m_{22}X_{t,\delta}N_{t,u} - m_{22}X_{t,u}N_{t,\delta} + m_{32}X_{t,u}Y_{t,\delta} - m_{32}X_{t,\delta}Y_{t,u}; \\ q_3 &= X_{t,u}Y_{t,v}N_{t,\delta} - X_{t,u}Y_{t,\delta}N_{t,v} - X_{t,v}Y_{t,u}N_{t,\delta} + X_{t,v}Y_{t,\delta}N_{t,u} + X_{t,\delta}Y_{t,u}N_{t,v} - X_{t,\delta}Y_{t,v}N_{t,u}. \end{aligned}$$

There is no straightforward way to solve equation 4.9 if the behaviour of $\Delta\delta$ is unknown. An attempt to solve the simplified equation can be made by ignoring the inertia of the rudder and hence defining a quasi-static "rudder efficiency coefficient" q_3/a_4 similar to the one present in [25]. However, since in the case of the wPCC, we already established that a_4 is close to or smaller than zero, this coefficient will often flip negative or approach infinity and has little physical meaning. It is also not immediately clear that the time derivatives of the rudder motion can be ignored when calculating the yaw motion. Therefore, a proportional control scheme with gain $G_1 = 0.3$ is used to ensure a stable yaw motion for all points of sail, thus ensuring a meaningful comparison between various operational points. The situation considered is a steady operational condition at equilibrium. Then a new target angle ψ_r is introduced at $t = 0$, hence the change in rudder angle will be equal to

$$\Delta\delta = G_1(\psi - \psi_r). \tag{4.10}$$

This way the control system aims for a yaw angle that differs from the previous yaw angle ψ_0 by the value ψ_r. The obtained solution can be interpreted as a step response to the combined rudder controller/ship-system.

Now $\Delta\delta$ can be written in terms of ψ so that the ODE can be solved. The new ODE containing only time derivatives of ψ, and divided by the reference angle ψ_r, looks like the following:

$$a_0 \frac{\dddot{r}(t)}{\psi_r} + a_1 \frac{\ddot{r}(t)}{\psi_r} + (a_2 - q_1G_1)\frac{\dot{r}(t)}{\psi_r} + (a_3 - q_2G_1)\frac{r(t)}{\psi_r} + (a_4 - q_3G_1)\frac{\psi(t)}{\psi_r} = -q_3G_1 \tag{4.11}$$

It turns out that the corresponding characteristic equation

$$a_0\lambda^4 + a_1\lambda^3 + (a_2 - q_1G_1)\lambda^2 + (a_3 - q_2G_1)\lambda + (a_4 - q_3G_1) = 0 \tag{4.12}$$

has two real roots and one pair of complex conjugates. After using familiar techniques for solving polynomial equations, these roots can be expressed in terms of the polynomial coefficients. In practical applications, a numerical root finding method suffices. The characteristic equation can be rewritten in its root form as follows:

$$a_0(\lambda - \tilde{\sigma}_0)(\lambda - \tilde{\sigma}_1)(\lambda - (\tilde{\sigma}_{2R} + \tilde{\sigma}_{2I}i))(\lambda - (\tilde{\sigma}_{2R} - \tilde{\sigma}_{2I}i)) = 0 \tag{4.13}$$

The general solution of the ODE then looks as follows:

$$\frac{\Delta\psi(t)}{\psi_r} = C_0e^{\tilde{\sigma}_0 t} + C_1e^{\tilde{\sigma}_1 t} + C_2e^{\tilde{\sigma}_{2R} t}\cos(\tilde{\sigma}_{2I}t) + C_3e^{\tilde{\sigma}_{2R} t}\sin(\tilde{\sigma}_{2I}t) + C_4 \tag{4.14}$$

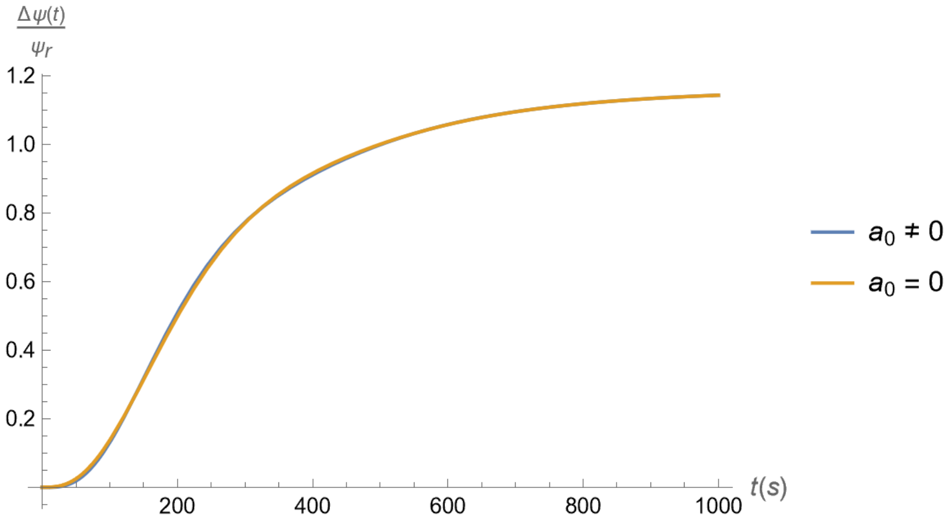

Figure 4.10: Comparison between yaw motion at $\theta_w = 50°$ with and without the approximation $a_0 = 0$.

The root $\tilde{\sigma}_0$, which is the root with the most negative real part, can be disregarded in the final solution since it is a solution component of relatively high frequency, which quickly approaches zero as $t > 0$. This is akin to making the simplification that $a_0 = 0$, which is an inertia term that is neglected in the K-T Nomoto model as well [14]. It turns out this simplification does not change the other coefficients by much, as exemplified by numerically solving the yaw motion for $\theta_w = 50°$ both with and without this approximation. The result is visible in Figure 4.10.
The simplified ODE characteristic equation can now be summarised as follows:

$$a_1\lambda^3 + (a_2 - q_1G_1)\lambda^2 + (a_3 - q_2G_1)\lambda + (a_4 - q_3G_1) = 0 \tag{4.15}$$

$$a_1(\lambda - \sigma_1)(\lambda - (\sigma_{2R} + \sigma_{2I}i))(\lambda - (\sigma_{2R} - \sigma_{2I}i)) = 0 \tag{4.16}$$

$$\frac{\Delta\psi(t)}{\psi_r} = C_1e^{\sigma_1 t} + C_2e^{\sigma_{2R}t}\cos(\sigma_{2I}t) + C_3e^{\sigma_{2R}t}\sin(\sigma_{2I}t) + C_4 \tag{4.17}$$

The chosen boundary conditions are $\frac{\psi(\infty)}{\psi_r} = \frac{-q_3G_1}{a_4 - q_3G_1}$ (assuming that all time derivatives converge to zero, this is the static solution at infinity), $\psi(0) = 0$, $r(0) = 0$, $\dot{r}(0) = 0$, and $\ddot{r}(0) = 0$. These boundary conditions represent a situation in which the ODE is completely solvable, and the lowest-order time derivatives of the yaw angle are zero at $t = 0$. This leads to the following linear system of boundary equations:

$$\begin{bmatrix} 0 \\ 0 \\ 0 \\ \frac{-q_3G_1}{a_4 - q_3G_1} \end{bmatrix} = \begin{bmatrix} 1 & 1 & 0 & 1 \\ \sigma_1 & \sigma_{2R} & \sigma_{2I} & 0 \\ \sigma_1^2 & \sigma_{2R}^2 - \sigma_{2I}^2 & 2\sigma_{2R}\sigma_{2I} & 0 \\ 0 & 0 & 0 & 1 \end{bmatrix} \begin{bmatrix} C_1 \\ C_2 \\ C_3 \\ C_4 \end{bmatrix} \tag{4.18}$$

This linear system can now be solved to obtain the boundary coefficients by inverting the matrix on the right hand side. The result is a convoluted expression of terms appearing in Equation 4.18 and can be easily calculated by inverting the matrix.

When examining the solution for three different points of sail (closed-hauled, beam reach and broad reach), it becomes clear that the oscillatory components driven by σ_{2R} and σ_{2I} have a relatively small contribution to the motion. The numerical values of the solution coefficients are presented in Table 4.1.

The solutions, normalised by the reference angle ψ_r, are dominated by the real eigenvalue σ_1. Oscillatory components are virtually negligible. Yaw oscillation, which was the dominant phenomenon in the last section of the previous work by Yasukawa et. al [25], driven by the complex conjugate pair of eigenvalues σ_2, plays almost no role here due to the additional eigenvalue σ_1 dominating the transient response. The steady errors in the yaw response arise due to the fact that no integral control was applied. Whenever $a_4 \neq 0$, the steady error will be unequal to zero.

	$\theta_w = 50°$	$\theta_w = 90°$	$\theta_w = 130°$
σ_1	-0.00449485	-0.00538884	-0.00477033
σ_{2R}	-0.0105731	-0.0113001	-0.00776853
σ_{2I}	0.0145206	0.0157717	0.0114955
C_1	-1.51065	-1.41765	-1.40152
C_2	0.35044	0.349288	0.373944
C_3	-0.212452	-0.234121	-0.328886
C_4	1.16022	1.06836	1.02758

Table 4.1: Numerical values of coefficients of ODE solution for three different points of sail, using the human control scheme and the linear stable hull

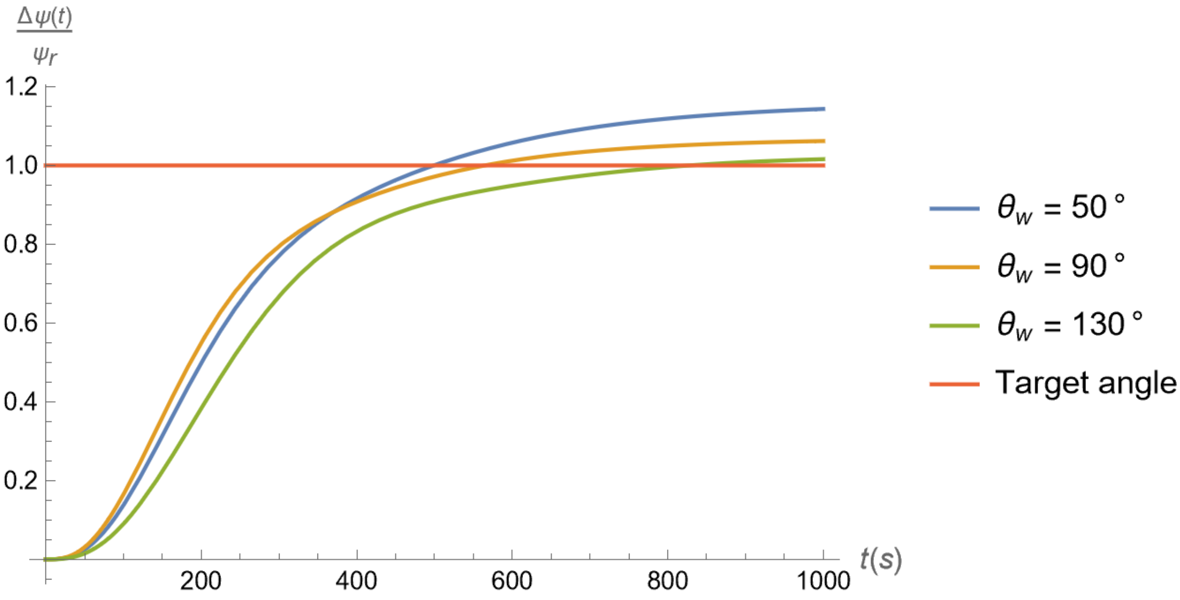

Figure 4.11: Time evolution of ODE solution for three different points of sail, using the human control scheme and the linear stable hull.

The autopilot control scheme gives an even better response, as can be seen both in the numerical overview in Table 4.2 and the time response plot in Figure 4.12. The steady error is a lot smaller, owing to the larger proportional gain applied in this case. Note that a proportional gain of 1.0 is still very reasonable in an actual operational context in the terms of actuator limits, as this means that the extra rudder angle applied is equal to the current yaw angle anomaly (not counting derivative gain).

Both the human and autopilot control cases show that the vessel from the case study is very controllable by active steering.

	$\theta_w = 50°$	$\theta_w = 90°$	$\theta_w = 130°$
σ_1	-0.0047302	-0.00538429	-0.00481328
σ_{2R}	-0.018626	-0.020248	-0.014127
σ_{2I}	0.0276442	0.0295592	0.0209084
C_1	-1.21086	-1.19565	-1.22522
C_2	0.167642	0.176081	0.217105
C_3	-0.0942371	-0.0971766	-0.135366
C_4	1.04322	1.01957	1.00812

Table 4.2: Numerical values of coefficients of ODE solution for three different points of sail, using the autopilot control scheme and the linear stable hull

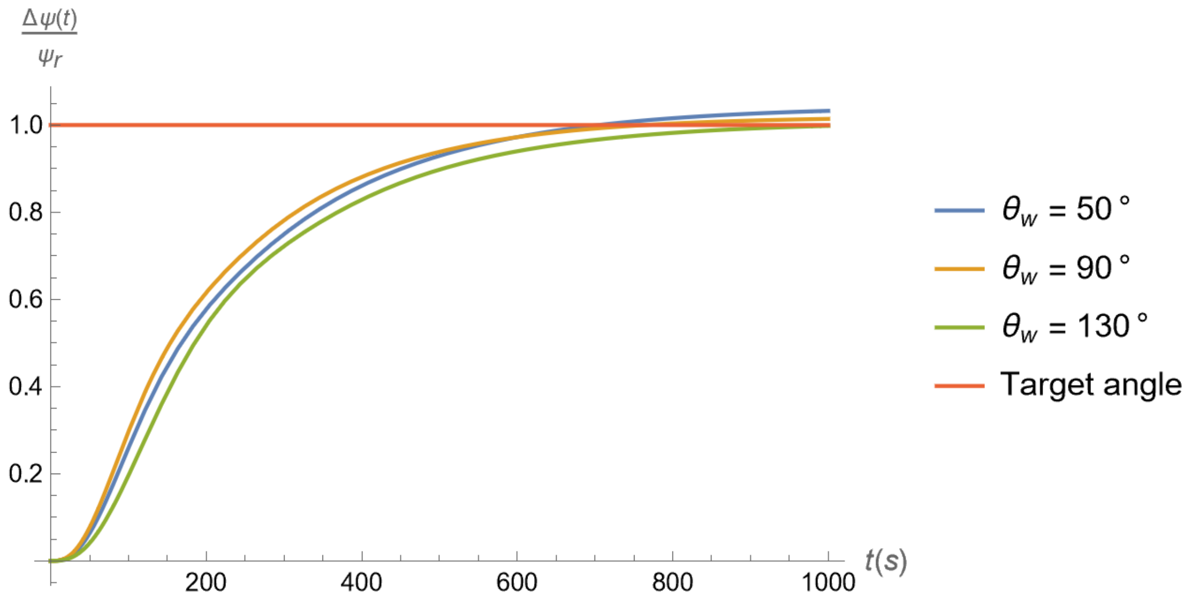

Figure 4.12: Time evolution of ODE solution for three different points of sail, using the autopilot control scheme and the linear stable hull.

5 Conclusions

We recall the research questions here:

To what extent is a vessel able to maintain yaw stability under the influence of varying wind conditions and control system specifications when introducing large aerodynamic control surfaces?

1. Which analytical methods can be used to assess the directional stability of vessels equipped with large aerodynamic control surfaces?
2. How do different modelling approaches impact the directional stability assessment of vessels?
3. How does the yaw motion of the system behave in both the frequency domain and the time domain under proportional and derivative feedback control strategies?

5.1. Analytical method

An analytical method was developed for assessing directional stability of any vessel for which the basic aerodynamic and hydrodynamic characteristics are known. The main aim when attacking the first research question was to mathematically reformulate the notion of a stable linearised system into a single inequality that holistically described the stability type of the system. Although this reduction of stability conditions turned out to be possible for this particular vessel, that is a tentative conclusion that might lose its value when the hydrodynamic coefficients look wholly different. Possible future work could look into examining the signs of the various Δ_i for a range of vessels.

For many practical applications, the easiest approach to assessing stability might be to directly derive the degree of instability of the system from the system matrices. This can be done by filling in the force derivative matrices with difference quotients to approximate the total derivative, exactly as demonstrated in this thesis with the SEAMAN data.

The directional stability diagnostic, whether in the form of a numerically-calculated DOI or an equivalent combination of Hurwitz coefficients, is a binary dimensionless quantity that could be expanded into a red/orange/green partition or similar. To do this, a notion of marginal stability would need to be defined, which could relate to the necessary gains needed to stabilise the system. This could be an interesting direction for future research in the field.

5.2. Model variations

The different model approaches that were performed provided various useful insights. Variations were made in the hydrodynamic parameters, the aerodynamic model, and the system dimension (whether to take into account surge coupling or not).

The different datasets for the hydrodynamic coefficients produced no significant results when comparing a nonlinear hull with a linear hull, at least for the original stable case. This is good news for the simple methods developed here, since the stability diagnostic should be invariant under the choice of hydrodynamic model. The fact that differences in the results arose for the artificially destabilised hulls can be explained by the relative importance of the linear coefficients (which are the coefficients that were altered), which is lower in the nonlinear model than in the linear one.

The effect of including a boundary layer in the wind model was also examined, mostly with the aim of improving the computational time of both the VPP algorithm and calculating the force derivatives. The differences in the stability outcome are almost completely negligible in this case, although this could change when sail-sail and wind-sail interaction effects are present in the force model. The computational effort is much larger for the boundary layer model, which requires the calculation of the apparent wind angle and speed at all sail heights instead of just once.

Surge coupling is perhaps the most interesting phenomenon here, since it has the strongest connection to the core of the research gap. Where previous directional stability models were able to disregard surge or even yaw angle - in the classical stability criterion, only sway and yaw *velocities* play a role - this thesis needed a state-space model of all four dimensions. The surge coupling effects turn out to not be negligible, although for some points of sail the differences are small. It could be expected that this dimension plays a stronger role in this case, since wind propulsion inevitably has a strong effect on the surge forces so that coupling effects are very likely in most situations.

5.3. Closed-loop analysis

When looking at the closed-loop response of the wPCC vessel, both a proportional gain scheme ($G_1 = 0.3, G_2 = 0.0$) and a PD scheme ($G_1 = 1.0, G_2 = 1.0$) were applied, corresponding to human control and autopilot control, respectively. The degree of instability (DOI) is then calculated with the closed-loop system matrix $\mathbf{A} - \mathbf{BK}$. The DOI values for both control schemes are satisfactory on all points of sail when looking at the original hull. For the artificially destabilised hulls the results are, in varying degrees, relatively more unstable - as expected. Again, the SEAMAN data serve as a verification for the stable hull results.

The time-domain response of a step rudder input was also solved. This was done by first neglecting the most high-frequency eigenvalue through the approximation $a_0 = 0$, and then applying the boundary conditions $\psi(0) = r(0) = \dot{r}(0) = 0$ on the resulting third-degree ODE. Numerical solutions for three different points of sail yielded small steady errors and negligible oscillatory components for the human steering control scheme, and yielded negligible steady errors and negligible oscillatory components for the autopilot control scheme.

Most solutions are dominated by the exponential term corresponding to the constant C_1 and the eigenvalue σ_1, which is the eigenvalue that arises due to the extra surge coupling term. When comparing the found results with a similar analysis done by Yasukawa et al. [25], the most striking difference is the absence of this eigenvalue in their work. As such, a comparison of the various eigenperiods of the oscillatory components has much less value in the present case.

The general conclusion is that, looking at the case study at hand, the wPCC vessel becomes directionally stable rather easily under active rudder control schemes, even when using moderate gain values and simple PD control. The step responses are acceptable in the time domain when looking at overshoot. For a more realistic estimation of the response (especially the settling time which is at present quite long), the rudder action should be driven by a maximum rudder angle rate $\dot{\delta}$ or even a separate plant including rudder inertia. In the current analysis, the chosen boundary conditions may diverge from reality because they were rather conservative.

5.4. Future work

Future work done in the field might build on this research in the following ways:

- Expand the motion model to a 4DOF model, adding roll (ϕ) and roll rate (p) as variables. This would imply that the state-space model has six dimensions, and the ODE would become even more complex. However, numerical directional stability assessments with respect to a varying wind speed and subsequent heeling effects could be interesting from both design and operational points of view;

- Explore the wind-assisted case (wingsail/Flettner/kite) where a propeller guarantees a steady ship speed;
- Evaluate sheeting control strategies (especially multiple sails). Note that the notation from this thesis already facilitates the use of sheeting angles as input variables, which was briefly explored and then abandoned due to unverifiable results;
- Develop traffic-light diagnostic (stable/marginally stable/unstable) or similar;
- Examine fundamentally different hull shapes like tankers, container vessels, and small sailing yachts;
- Experimentally validate methodology using existent scale models;
- Compare different underlying models:
  - High-fidelity methods like turbulence models, flow-sail and sail-sail interaction;
  - Integral control gain;
  - Alternative hydrodynamic models like the MMG model [24];
- Find general sign of Δ_2, Δ_3 for a wide variety of vessels to reduce the conditions for stability.

References

[1] Martin A Abkowitz. *Lectures on Ship Hydrodynamics - Steering and Manoeuvrability*. 1964.

[2] Manolis Angelou and Kostas J Spyrou. *A New Mathematical Model for Investigating Course Stability and Maneuvering Motions of Sailing Yachts*. 2017.

[3] Katherine Calvin et al. *Climate Change 2023 - Synthesis Report*. Ed. by Paola Arias et al. July 2023. DOI: `10.59327/IPCC/AR6-9789291691647`.

[4] Kenneth S. M. Davidson and Leonard I. Schiff. “Turning and Course-Keeping Qualities”. In: *SNAME Transactions* (1946).

[5] Shiyu Deng and Zhifu Mi. “A review on carbon emissions of global shipping”. In: *Marine Development* 1 (1 Nov. 2023). DOI: `10.1007/s44312-023-00001-2`.

[6] Haruzo Eda. “Low-speed controllability of ships in wind”. In: *Journal of Ship Research* 12 (03 1968), pp. 181–200.

[7] Thor I. Fossen. *Handbook of marine craft hydrodynamics and motion control*. Wiley, 2011, p. 596. ISBN: 9781119991496.

[8] Thor I. Fossen and Trygve Lauvdal. “Nonlinear Stability Analysis of Ship Autopilots in Sway, Roll and Yaw”. In: 1994, pp. 113–124.

[9] Masayoshi Hirano and Junshi Takashina. *A Calculation of Ship Turning Motion Taking Coupling Effect Due to Heel into Consideration*. Mar. 1980.

[10] IMO. *Strategy on Reduction of GHG Emissions from Ships*. 2023.

[11] Katsuro Kijima et al. “On the Manoeuvring Performance of a Ship with the Parameter of Loading Condition”. In: *Journal of the Society of Naval Architects of Japan* 168 (1990), pp. 141–148.

[12] Martin Kjellberg, Frederik Gerhardt, and Sofia Werner. “Sailing Performance of Wind-Powered Cargo Vessel in Unsteady Conditions”. In: *Journal of Sailing Technology* 8 (1 2023), pp. 218–254.

[13] Kensaku Nomoto and Kyoung-Ho Son. “On the Coupled Motion of Steering and Rolling of a High-Speed Container Ship”. In: *Journal of the Society of Naval Architects of Japan* 150 (1981), pp. 232–244.

[14] Kensaku Nomoto and Kenshi Taguchi. “On steering qualities of ships”. In: *Journal of Zosen Kiokai* 1957 (101 1957), pp. 57–66.

[15] Fredrik Olsson, Laura Marimon Giovannetti, and Christian Finnsgård. “A Performance Depowering Investigation for Wind Powered Cargo Ships Along a Route”. In: *Journal of Sailing Technology* 5 (1 2020), pp. 47–60.

[16] Panos Y Papalambros and Douglass J Wilde. *Principles of optimal design: modeling and computation*. Cambridge university press, 2000.

[17] Svein I Sagatun and Thor I Fossen. “Lagrangian formulation of underwater vehicles’ dynamics”. In: *Conference Proceedings 1991 IEEE International Conference on Systems, Man, and Cybernetics* (1991), pp. 1029–1034.

[18] R. Rajita Shenoi, P. Krishnankutty, and R. Panneer Selvam. “Sensitivity Study of Hydrodynamic Derivative Variations on the Maneuverability Prediction of a Container Ship”. In: American Society of Mechanical Engineers, 2015.

[19] Salma Sherbaz and Wenyang Duan. “Operational options for green ships”. In: *Journal of Marine Science and Application* 11 (3 Sept. 2012), pp. 335–340. ISSN: 16719433. DOI: `10.1007/s11804-012-1141-2`.

[20] Kostas Spyrou. “Yaw stability of ships in steady wind”. In: *Ship Technology Research* 42 (1 1995), pp. 21–30.

[21] Serge Sutulo and C. Guedes Soares. *Mathematical models for simulation of manoeuvring performance of ships*. 2011.

[22] *The Oceanbird Concept*. Mar. 2024. URL: https://www.theoceanbird.com/the-oceanbird-concept/.

[23] Ioannis G. Tigkas. "Nonlinear Dynamic Analysis of the Course Instability of Ships in Wind and Waves". In: (2010).

[24] H. Yasukawa and Y. Yoshimura. "Introduction of MMG standard method for ship maneuvering predictions". In: *Journal of Marine Science and Technology (Japan)* 20 (1 Mar. 2015), pp. 37–52. ISSN: 09484280. DOI: 10.1007/s00773-014-0293-y.

[25] H. Yasukawa et al. "Course stability and yaw motion of a ship in steady wind". In: *Journal of Marine Science and Technology (Japan)* 17 (3 Apr. 2012), pp. 291–304. ISSN: 09484280. DOI: 10.1007/s00773-012-0168-z.

[26] Hironori Yasukawa and Ryoya Sakuno. "Application of the MMG method for the prediction of steady sailing condition and course stability of a ship under external disturbances". In: *Journal of Marine Science and Technology* 25 (2020), pp. 196–220.

A

Intermediate VPP results

Table A.1: VPP results for linear stable hull

θ_W (°)	u_0 (m/s)	v_0 (m/s)	δ_0 (°)	$\alpha_{0,1}$ (°)	$\alpha_{0,2}$ (°)	$\alpha_{0,3}$ (°)	$\alpha_{0,4}$ (°)
32	5.76549	-1.01705	3.49014	18.2875	18.2571	18.2268	18.1967
33	5.90448	-1.00977	3.34924	18.3996	18.4265	18.4523	18.477
34	6.0391	-1.00033	3.22079	18.4486	18.4697	18.49	18.5097
35	6.1696	-0.991146	3.1011	18.493	18.5093	18.525	18.5404
36	6.29612	-0.982177	2.98929	18.5334	18.5457	18.5576	18.5693
37	6.41878	-0.973392	2.88457	18.5704	18.5793	18.588	18.5966
38	6.53768	-0.964761	2.78626	18.6045	18.6105	18.6165	18.6225
39	6.65292	-0.956259	2.69375	18.6359	18.6396	18.6433	18.647
40	6.76457	-0.947862	2.60652	18.6651	18.6668	18.6685	18.6702
41	6.87271	-0.93955	2.52408	18.6923	18.6923	18.6923	18.6923
42	6.97739	-0.931307	2.44604	18.7179	18.7165	18.7151	18.7137
43	7.07837	-0.923108	2.37198	18.7419	18.7395	18.7371	18.7347
44	7.17564	-0.914931	2.30158	18.7646	18.7613	18.758	18.7547
45	7.26923	-0.906762	2.23451	18.786	18.782	18.7779	18.7738
46	7.35921	-0.89859	2.17053	18.8063	18.8016	18.7969	18.7921
47	7.44562	-0.890405	2.10937	18.8256	18.8203	18.815	18.8096
48	7.52848	-0.882197	2.05082	18.8439	18.8382	18.8324	18.8265
49	7.60785	-0.873958	1.99469	18.8613	18.8552	18.849	18.8427
50	7.68375	-0.865682	1.9408	18.878	18.8716	18.865	18.8583
51	7.75621	-0.857362	1.88898	18.894	18.8872	18.8804	18.8734
52	7.82526	-0.848992	1.83909	18.9093	18.9023	18.8952	18.8879
53	7.89093	-0.840568	1.791	18.924	18.9168	18.9094	18.902
54	7.95324	-0.832086	1.74458	18.9382	18.9308	18.9232	18.9156
55	8.0122	-0.823543	1.69972	18.9518	18.9443	18.9366	18.9287
56	8.06785	-0.814935	1.65632	18.965	18.9573	18.9495	18.9415
57	8.12021	-0.80626	1.6143	18.9777	18.97	18.962	18.9539
58	8.16928	-0.797516	1.57355	18.9901	18.9822	18.9742	18.966
59	8.2151	-0.788701	1.534	19.002	18.9941	18.986	18.9777
60	8.25792	-0.779815	1.49541	19.0135	19.0054	18.9971	18.9886
61	8.29816	-0.770861	1.45746	19.0246	19.0163	19.0078	18.9991
62	8.33582	-0.76184	1.4201	19.0354	19.0269	19.0182	19.0093
63	8.37092	-0.752753	1.3833	19.0459	19.0373	19.0284	19.0193
64	8.40347	-0.743601	1.34701	19.0562	19.0474	19.0384	19.0291
65	8.43347	-0.734385	1.31121	19.0661	19.0572	19.0481	19.0387
66	8.46093	-0.725105	1.27586	19.0759	19.0669	19.0576	19.0481
67	8.48588	-0.715764	1.24094	19.0854	19.0763	19.0669	19.0573

θ_W (°)	u_0 (m/s)	v_0 (m/s)	δ_0 (°)	$\alpha_{0,1}$ (°)	$\alpha_{0,2}$ (°)	$\alpha_{0,3}$ (°)	$\alpha_{0,4}$ (°)
68	8.50832	-0.706362	1.2064	19.0947	19.0855	19.076	19.0663
69	8.52826	-0.696901	1.17224	19.1038	19.0945	19.085	19.0751
70	8.54572	-0.687383	1.13841	19.1127	19.1033	19.0937	19.0838
71	8.56072	-0.677811	1.10489	19.1214	19.112	19.1023	19.0923
72	8.57326	-0.668185	1.07166	19.13	19.1205	19.1108	19.1007
73	8.58337	-0.658509	1.0387	19.1384	19.1289	19.1191	19.109
74	8.59107	-0.648784	1.00598	19.1466	19.1371	19.1273	19.1171
75	8.59636	-0.639014	0.973475	19.1547	19.1452	19.1353	19.1251
76	8.59919	-0.629183	0.941261	19.1628	19.1532	19.1433	19.1332
77	8.59931	-0.619241	0.909559	19.1707	19.1611	19.1513	19.1412
78	8.59675	-0.609188	0.878358	19.1785	19.169	19.1592	19.1491
79	8.59152	-0.599027	0.847632	19.1862	19.1767	19.167	19.1569
80	8.58366	-0.588759	0.817358	19.1938	19.1844	19.1746	19.1646
81	8.57319	-0.57839	0.787513	19.2013	19.1919	19.1822	19.1723
82	8.56015	-0.56792	0.758075	19.2087	19.1994	19.1898	19.1798
83	8.54456	-0.557355	0.729024	19.216	19.2068	19.1972	19.1873
84	8.52646	-0.546696	0.70034	19.2233	19.2141	19.2046	19.1948
85	8.50588	-0.535948	0.672006	19.2305	19.2214	19.2119	19.2021
86	8.48287	-0.525114	0.644002	19.2377	19.2285	19.2191	19.2094
87	8.45746	-0.514196	0.616314	19.2448	19.2357	19.2263	19.2167
88	8.42968	-0.5032	0.588924	19.2518	19.2428	19.2335	19.2239
89	8.39959	-0.492128	0.561828	19.2588	19.2498	19.2406	19.231
90	8.36745	-0.480974	0.536004	19.2657	19.2567	19.2475	19.238
91	8.33346	-0.469734	0.512106	19.2725	19.2636	19.2544	19.245
92	8.29767	-0.458412	0.49015	19.2793	19.2704	19.2613	19.2519
93	8.26011	-0.447013	0.470151	19.286	19.2772	19.2681	19.2587
94	8.22084	-0.435542	0.452126	19.2927	19.2839	19.2749	19.2656
95	8.17991	-0.424003	0.436096	19.2993	19.2906	19.2816	19.2724
96	8.13738	-0.412404	0.422087	19.3059	19.2972	19.2883	19.2792
97	8.09328	-0.400742	0.410118	19.3124	19.3038	19.295	19.2859
98	8.04767	-0.389026	0.400219	19.3189	19.3104	19.3017	19.2927
99	8.0006	-0.377261	0.392423	19.3254	19.317	19.3083	19.2994
100	7.95213	-0.365449	0.386732	19.3319	19.3235	19.3149	19.3061
101	7.90217	-0.353595	0.381421	19.3383	19.33	19.3216	19.3129
102	7.85068	-0.341701	0.375461	19.3448	19.3366	19.3282	19.3196
103	7.79774	-0.329771	0.368832	19.3512	19.3431	19.3349	19.3264
104	7.74339	-0.317809	0.361514	19.3577	19.3497	19.3415	19.3331
105	7.68772	-0.305818	0.353487	19.3642	19.3562	19.3481	19.3398
106	7.63078	-0.293802	0.344728	19.3707	19.3628	19.3547	19.3465
107	7.57264	-0.281765	0.335216	19.3772	19.3694	19.3614	19.3532
108	7.51336	-0.269711	0.324926	19.3838	19.376	19.368	19.3599
109	7.453	-0.257641	0.313874	19.3903	19.3826	19.3747	19.3667
110	7.39115	-0.245559	0.303456	19.3969	19.3893	19.3815	19.3735
111	7.32764	-0.233468	0.294397	19.4036	19.396	19.3883	19.3804
112	7.26255	-0.221366	0.286746	19.4103	19.4028	19.3951	19.3874
113	7.19596	-0.209254	0.280556	19.417	19.4096	19.402	19.3944
114	7.12794	-0.197132	0.275883	19.4238	19.4165	19.409	19.4014
115	7.05859	-0.184998	0.272792	19.4307	19.4234	19.416	19.4085
116	6.98798	-0.172851	0.27135	19.4376	19.4303	19.423	19.4156
117	6.91642	-0.160827	0.270299	19.4445	19.4373	19.4301	19.4227
118	6.84433	-0.149137	0.267565	19.4515	19.4444	19.4372	19.4299
119	6.77179	-0.137786	0.263072	19.4586	19.4515	19.4443	19.437
120	6.69888	-0.126773	0.256764	19.4658	19.4587	19.4515	19.4443
121	6.62564	-0.116097	0.248581	19.473	19.4659	19.4587	19.4515
122	6.55216	-0.105757	0.238463	19.4803	19.4732	19.466	19.4589

θ_W (°)	u_0 (m/s)	v_0 (m/s)	δ_0 (°)	$\alpha_{0,1}$ (°)	$\alpha_{0,2}$ (°)	$\alpha_{0,3}$ (°)	$\alpha_{0,4}$ (°)
123	6.47842	-0.095688	0.226554	19.4877	19.4806	19.4734	19.4663
124	6.40427	-0.0857206	0.21334	19.4952	19.4881	19.4809	19.4737
125	6.32976	-0.0758424	0.198793	19.5028	19.4957	19.4885	19.4813
126	6.25497	-0.0660487	0.182854	19.5106	19.5034	19.4962	19.489
127	6.17994	-0.0563339	0.165459	19.5184	19.5112	19.5039	19.4967
128	6.10465	-0.0466863	0.146766	19.5265	19.5191	19.5119	19.5046
129	6.02822	-0.0370424	0.129032	19.5346	19.5273	19.5199	19.5126
130	5.95046	-0.0273734	0.112927	19.543	19.5356	19.5282	19.5208
131	5.8714	-0.0176613	0.0985582	19.5516	19.5441	19.5366	19.5292
132	5.79106	-0.00788532	0.0860506	19.5603	19.5528	19.5453	19.5378
133	5.71083	0.00183012	0.0750155	19.5693	19.5616	19.554	19.5465
134	5.63427	0.0111161	0.0641327	19.5783	19.5705	19.5628	19.5552
135	5.56131	0.0199696	0.0533642	19.5874	19.5794	19.5716	19.5639
136	5.49171	0.0284066	0.0427468	19.5965	19.5885	19.5806	19.5727
137	5.42512	0.0364622	0.0320383	19.6058	19.5976	19.5896	19.5817
138	5.36031	0.044347	0.018575	19.6154	19.607	19.5988	19.5907
139	5.29693	0.0521171	0.00166304	19.6251	19.6165	19.6081	19.5999
140	5.23494	0.0597779	-0.0187278	19.6351	19.6263	19.6177	19.6093
141	5.17428	0.0673357	-0.042563	19.6454	19.6364	19.6275	19.6189
142	5.11389	0.0748299	-0.066684	19.656	19.6467	19.6376	19.6287
143	5.05323	0.0822903	-0.0893086	19.667	19.6574	19.6479	19.6388
144	4.9923	0.0897304	-0.110354	19.6785	19.6684	19.6587	19.6492
145	4.93111	0.0971668	-0.129726	19.6904	19.6799	19.6698	19.66
146	4.8697	0.1047	-0.147331	19.7027	19.6918	19.6813	19.6711
147	4.80807	0.112394	-0.163052	19.7156	19.7043	19.6933	19.6827
148	4.74622	0.120269	-0.176739	19.7291	19.7172	19.7058	19.6948
149	4.68405	0.12832	-0.188416	19.7432	19.7307	19.7187	19.7072
150	4.62102	0.136343	-0.199664	19.7581	19.7449	19.7322	19.7202
151	4.55695	0.144309	-0.2108	19.7737	19.7597	19.7464	19.7337
152	4.49177	0.152242	-0.221729	19.7903	19.7754	19.7613	19.7478
153	4.42624	0.160206	-0.235776	19.808	19.7922	19.7773	19.7632
154	4.36198	0.168299	-0.259931	19.8268	19.8101	19.7943	19.7793
155	4.29887	0.176538	-0.294853	19.8469	19.829	19.8121	19.7963
156	4.23679	0.18494	-0.340815	19.8684	19.849	19.8308	19.8138
157	4.17446	0.193693	-0.392616	19.8912	19.8699	19.8501	19.8316
158	4.11126	0.202911	-0.448353	19.9158	19.8924	19.8706	19.8504
159	4.0471	0.212639	-0.508458	19.9425	19.9164	19.8924	19.8703
160	3.98191	0.222896	-0.575571	19.9715	19.9423	19.9156	19.8912

Table A.2: VPP results for nonlinear stable hull

θ_W (°)	u_0 (m/s)	v_0 (m/s)	δ_0 (°)	$\alpha_{0,1}$ (°)	$\alpha_{0,2}$ (°)	$\alpha_{0,3}$ (°)	$\alpha_{0,4}$ (°)
32	5.95021	-1.00877	3.48155	18.3809	18.4629	18.5346	18.598
33	6.07886	-1.0063	3.33362	18.4308	18.5015	18.5643	18.6203
34	6.20396	-1.00355	3.19616	18.476	18.5372	18.5921	18.6418
35	6.32558	-1.00053	3.06812	18.5171	18.5702	18.6184	18.6623
36	6.44378	-0.997245	2.94854	18.5548	18.6009	18.6432	18.6821
37	6.55863	-0.993714	2.83663	18.5894	18.6295	18.6667	18.7011
38	6.67018	-0.989942	2.73165	18.6215	18.6564	18.689	18.7194
39	6.77849	-0.985939	2.63296	18.6512	18.6816	18.7102	18.7371
40	6.8836	-0.98171	2.54001	18.6789	18.7053	18.7304	18.7541
41	6.98553	-0.977261	2.45229	18.7048	18.7278	18.7496	18.7705
42	7.08434	-0.972598	2.36936	18.7291	18.749	18.7681	18.7863
43	7.17996	-0.967725	2.29082	18.7521	18.7694	18.786	18.802

θ_W (°)	u_0 (m/s)	v_0 (m/s)	δ_0 (°)	$\alpha_{0,1}$ (°)	$\alpha_{0,2}$ (°)	$\alpha_{0,3}$ (°)	$\alpha_{0,4}$ (°)
44	7.27218	-0.962629	2.21629	18.7738	18.7889	18.8034	18.8175
45	7.36098	-0.957314	2.14544	18.7944	18.8075	18.8201	18.8324
46	7.44639	-0.951782	2.07797	18.814	18.8252	18.8362	18.8469
47	7.52845	-0.946039	2.01361	18.8326	18.8422	18.8517	18.8609
48	7.60716	-0.940087	1.95214	18.8503	18.8585	18.8666	18.8745
49	7.68255	-0.933931	1.89331	18.8673	18.8742	18.881	18.8877
50	7.75465	-0.927573	1.83696	18.8835	18.8892	18.8949	18.9005
51	7.82347	-0.921017	1.78289	18.899	18.9038	18.9084	18.913
52	7.88902	-0.914267	1.73094	18.914	18.9177	18.9215	18.9252
53	7.95133	-0.907326	1.68097	18.9283	18.9313	18.9342	18.937
54	8.0104	-0.900198	1.63284	18.9422	18.9443	18.9465	18.9486
55	8.06626	-0.892885	1.58643	18.9556	18.957	18.9584	18.9598
56	8.11891	-0.88539	1.54163	18.9685	18.9693	18.9701	18.9709
57	8.16837	-0.877718	1.49833	18.981	18.9812	18.9814	18.9816
58	8.21466	-0.869871	1.45644	18.9931	18.9928	18.9925	18.9921
59	8.25779	-0.861853	1.41587	19.0049	19.004	19.0032	19.0024
60	8.29777	-0.853667	1.37655	19.0163	19.015	19.0137	19.0124
61	8.33499	-0.845322	1.33813	19.0272	19.0254	19.0236	19.0217
62	8.36973	-0.836829	1.30039	19.0379	19.0356	19.0332	19.0308
63	8.40199	-0.828191	1.26328	19.0483	19.0455	19.0426	19.0397
64	8.43178	-0.819412	1.22676	19.0584	19.0551	19.0518	19.0485
65	8.45911	-0.810495	1.19079	19.0683	19.0646	19.0609	19.0571
66	8.48399	-0.801445	1.15534	19.0779	19.0738	19.0697	19.0655
67	8.50643	-0.792264	1.12038	19.0874	19.0829	19.0784	19.0738
68	8.52644	-0.782958	1.08587	19.0966	19.0918	19.0869	19.082
69	8.54404	-0.77353	1.05178	19.1056	19.1005	19.0953	19.09
70	8.55923	-0.763984	1.01809	19.1144	19.109	19.1035	19.0979
71	8.57202	-0.754324	0.984755	19.1231	19.1174	19.1116	19.1057
72	8.58245	-0.744555	0.951761	19.1316	19.1256	19.1196	19.1134
73	8.59051	-0.734679	0.91908	19.1399	19.1337	19.1275	19.121
74	8.59622	-0.724703	0.886687	19.1481	19.1417	19.1352	19.1285
75	8.59961	-0.714629	0.854558	19.1562	19.1496	19.1428	19.1359
76	8.60069	-0.704463	0.822673	19.1641	19.1573	19.1504	19.1433
77	8.59925	-0.694159	0.791232	19.172	19.1651	19.158	19.1508
78	8.59516	-0.68369	0.760343	19.1797	19.1727	19.1655	19.1581
79	8.58847	-0.673061	0.72998	19.1874	19.1803	19.1729	19.1655
80	8.57919	-0.662275	0.70012	19.195	19.1877	19.1803	19.1727
81	8.56735	-0.651337	0.67074	19.2024	19.1951	19.1876	19.1799
82	8.55299	-0.640251	0.641818	19.2098	19.2024	19.1948	19.187
83	8.53615	-0.629021	0.613333	19.2171	19.2097	19.202	19.1941
84	8.51684	-0.617651	0.585267	19.2244	19.2168	19.2091	19.2011
85	8.49511	-0.606146	0.557602	19.2316	19.224	19.2161	19.2081
86	8.47099	-0.59451	0.530319	19.2387	19.231	19.2231	19.2151
87	8.44453	-0.582748	0.503404	19.2458	19.238	19.2301	19.222
88	8.41576	-0.570863	0.47684	19.2528	19.245	19.237	19.2288
89	8.38473	-0.558863	0.450616	19.2597	19.2519	19.2439	19.2356
90	8.3516	-0.546742	0.425234	19.2666	19.2587	19.2506	19.2423
91	8.31667	-0.534495	0.401838	19.2734	19.2655	19.2573	19.2489
92	8.28	-0.522127	0.380482	19.2802	19.2722	19.264	19.2555
93	8.24165	-0.509642	0.361183	19.2869	19.2788	19.2706	19.2621
94	8.20165	-0.497045	0.343961	19.2936	19.2855	19.2772	19.2686
95	8.16006	-0.484343	0.32884	19.3002	19.292	19.2837	19.2752
96	8.11693	-0.471542	0.315847	19.3067	19.2986	19.2903	19.2817
97	8.07231	-0.458642	0.305004	19.3132	19.3051	19.2968	19.2882
98	8.02625	-0.44565	0.296343	19.3197	19.3116	19.3032	19.2947

θ_W (°)	u_0 (m/s)	v_0 (m/s)	δ_0 (°)	$\alpha_{0,1}$ (°)	$\alpha_{0,2}$ (°)	$\alpha_{0,3}$ (°)	$\alpha_{0,4}$ (°)
99	7.97881	-0.432573	0.289899	19.3262	19.3181	19.3097	19.3011
100	7.93004	-0.419415	0.285706	19.3326	19.3245	19.3162	19.3076
101	7.87988	-0.40618	0.282355	19.3391	19.3309	19.3226	19.3141
102	7.82826	-0.39287	0.27842	19.3455	19.3374	19.3291	19.3206
103	7.77525	-0.379491	0.273884	19.3519	19.3438	19.3356	19.3271
104	7.72091	-0.366046	0.268729	19.3584	19.3503	19.3421	19.3336
105	7.6653	-0.352536	0.262936	19.3648	19.3568	19.3485	19.3401
106	7.60849	-0.338973	0.256488	19.3713	19.3632	19.355	19.3466
107	7.55055	-0.325358	0.249363	19.3778	19.3697	19.3615	19.3531
108	7.49155	-0.311694	0.241541	19.3843	19.3762	19.368	19.3596
109	7.43155	-0.29799	0.233029	19.3908	19.3827	19.3745	19.3661
110	7.37013	-0.284241	0.225192	19.3974	19.3893	19.3811	19.3728
111	7.30711	-0.270453	0.218823	19.404	19.396	19.3878	19.3795
112	7.24258	-0.256626	0.213975	19.4107	19.4027	19.3945	19.3863
113	7.17659	-0.242759	0.210703	19.4174	19.4094	19.4013	19.3931
114	7.10926	-0.228857	0.20907	19.4241	19.4161	19.4081	19.3999
115	7.04064	-0.214918	0.20914	19.4309	19.423	19.4149	19.4068
116	6.97083	-0.200938	0.210986	19.4378	19.4298	19.4218	19.4137
117	6.90013	-0.187084	0.21324	19.4446	19.4367	19.4287	19.4206
118	6.82894	-0.173596	0.213803	19.4516	19.4437	19.4357	19.4276
119	6.75733	-0.160479	0.212601	19.4586	19.4507	19.4427	19.4346
120	6.68535	-0.147736	0.209575	19.4657	19.4577	19.4497	19.4416
121	6.6131	-0.13537	0.204665	19.4729	19.4649	19.4568	19.4487
122	6.54059	-0.123376	0.197804	19.4801	19.4721	19.464	19.4558
123	6.46781	-0.111676	0.189181	19.4874	19.4794	19.4712	19.4631
124	6.39465	-0.10008	0.17933	19.4949	19.4867	19.4786	19.4704
125	6.32116	-0.0885771	0.168222	19.5024	19.4942	19.486	19.4778
126	6.2474	-0.0771618	0.155804	19.5101	19.5018	19.4935	19.4852
127	6.17343	-0.0658293	0.142015	19.5179	19.5095	19.5011	19.4928
128	6.09919	-0.0545663	0.12705	19.5258	19.5173	19.5089	19.5005
129	6.02383	-0.0432999	0.113194	19.5339	19.5253	19.5168	19.5083
130	5.94718	-0.0319992	0.10108	19.5421	19.5335	19.5249	19.5163
131	5.86925	-0.0206448	0.0908234	19.5506	19.5418	19.5331	19.5245
132	5.79008	-0.00921451	0.0825594	19.5592	19.5504	19.5416	19.5328
133	5.71105	0.00214451	0.0758436	19.5681	19.559	19.5501	19.5412
134	5.63561	0.0130051	0.0692026	19.5769	19.5677	19.5586	19.5497
135	5.56369	0.0233628	0.0625829	19.5859	19.5765	19.5673	19.5582
136	5.49503	0.0332346	0.0560126	19.5949	19.5853	19.576	19.5667
137	5.42934	0.0426568	0.0492885	19.6041	19.5943	19.5847	19.5754
138	5.36539	0.0518696	0.0398958	19.6134	19.6034	19.5937	19.5841
139	5.30286	0.060941	0.0271187	19.623	19.6128	19.6028	19.593
140	5.24169	0.0698762	0.0109264	19.6328	19.6223	19.6121	19.6021
141	5.18183	0.0786803	-0.00868703	19.6429	19.6321	19.6216	19.6114
142	5.12231	0.0873946	-0.0287998	19.6534	19.6422	19.6313	19.6208
143	5.06252	0.0960539	-0.0474043	19.6641	19.6525	19.6413	19.6305
144	5.00246	0.104672	-0.0644199	19.6753	19.6633	19.6517	19.6405
145	4.94213	0.113262	-0.0797527	19.6869	19.6744	19.6624	19.6508
146	4.88159	0.121928	-0.093277	19.699	19.686	19.6735	19.6615
147	4.82087	0.130749	-0.104858	19.7116	19.698	19.685	19.6725
148	4.75994	0.139741	-0.114355	19.7248	19.7105	19.6969	19.684
149	4.69875	0.148912	-0.121702	19.7385	19.7235	19.7093	19.6958
150	4.63677	0.15804	-0.128449	19.7529	19.7371	19.7222	19.708
151	4.57377	0.167058	-0.13513	19.768	19.7513	19.7356	19.7207
152	4.50969	0.175989	-0.141657	19.784	19.7663	19.7497	19.734
153	4.44496	0.184885	-0.150051	19.8012	19.7824	19.7649	19.7484

θ_W (°)	u_0 (m/s)	v_0 (m/s)	δ_0 (°)	$\alpha_{0,1}$ (°)	$\alpha_{0,2}$ (°)	$\alpha_{0,3}$ (°)	$\alpha_{0,4}$ (°)
154	4.38139	0.19386	-0.167857	19.8193	19.7995	19.781	19.7636
155	4.31899	0.202935	-0.196163	19.8387	19.8175	19.7978	19.7795
156	4.25767	0.212112	-0.235481	19.8594	19.8366	19.8156	19.7961
157	4.19646	0.221543	-0.281816	19.8813	19.8565	19.8337	19.8127
158	4.13445	0.231378	-0.331915	19.9049	19.8777	19.8529	19.8301
159	4.07158	0.241645	-0.386232	19.9304	19.9004	19.8732	19.8485
160	4.00775	0.252359	-0.44615	19.958	19.9248	19.8949	19.8679

Table A.3: VPP results for linear unstable hull

θ_W (°)	u_0 (m/s)	v_0 (m/s)	δ_0 (°)	$\alpha_{0,1}$ (°)	$\alpha_{0,2}$ (°)	$\alpha_{0,3}$ (°)	$\alpha_{0,4}$ (°)
32	5.67578	-0.880981	7.40058	18.043	18.239	18.3917	18.514
33	5.82216	-0.871993	7.13609	18.135	18.3024	18.436	18.545
34	5.96366	-0.863341	6.89042	18.2149	18.3591	18.4766	18.5741
35	6.10049	-0.854977	6.66163	18.2849	18.4101	18.514	18.6016
36	6.23288	-0.846859	6.44799	18.347	18.4564	18.5486	18.6274
37	6.36098	-0.838949	6.24798	18.4024	18.4985	18.5807	18.6519
38	6.48496	-0.831216	6.06027	18.4523	18.5372	18.6107	18.675
39	6.60493	-0.823631	5.88367	18.4974	18.5727	18.6387	18.697
40	6.72103	-0.816171	5.71717	18.5386	18.6056	18.665	18.718
41	6.83326	-0.808813	5.55987	18.5764	18.6365	18.6901	18.7384
42	6.94144	-0.80153	5.41101	18.6113	18.6653	18.714	18.7581
43	7.04565	-0.7943	5.26984	18.6436	18.6923	18.7366	18.7769
44	7.14596	-0.78711	5.1357	18.6736	18.7177	18.7579	18.7949
45	7.24244	-0.779944	5.00799	18.7015	18.7415	18.7782	18.8122
46	7.33515	-0.772791	4.88618	18.7277	18.764	18.7976	18.8287
47	7.42414	-0.76564	4.7698	18.7522	18.7853	18.816	18.8447
48	7.50948	-0.758483	4.65843	18.7753	18.8055	18.8336	18.86
49	7.5912	-0.75131	4.55168	18.7972	18.8246	18.8505	18.8747
50	7.66934	-0.744114	4.4492	18.8178	18.8429	18.8666	18.889
51	7.74394	-0.736889	4.35069	18.8374	18.8604	18.8822	18.9028
52	7.81504	-0.72963	4.25586	18.8561	18.8771	18.8971	18.9161
53	7.88266	-0.722332	4.16445	18.8738	18.8931	18.9115	18.929
54	7.94683	-0.71499	4.07623	18.8908	18.9085	18.9254	18.9416
55	8.00759	-0.707601	3.99099	18.9071	18.9233	18.9388	18.9537
56	8.06496	-0.700162	3.90853	18.9226	18.9375	18.9518	18.9655
57	8.11896	-0.692671	3.82866	18.9376	18.9512	18.9644	18.977
58	8.16961	-0.685124	3.75122	18.952	18.9645	18.9766	18.9882
59	8.21715	-0.67752	3.67586	18.9658	18.9771	18.988	18.9987
60	8.26202	-0.669862	3.60209	18.979	18.9892	18.9991	19.0088
61	8.30422	-0.662149	3.5298	18.9918	19.001	19.0099	19.0186
62	8.34378	-0.654382	3.4589	19.0042	19.0124	19.0204	19.0283
63	8.3807	-0.646561	3.38932	19.0162	19.0235	19.0307	19.0377
64	8.415	-0.638686	3.32097	19.0278	19.0343	19.0407	19.0469
65	8.44668	-0.630757	3.25379	19.0391	19.0448	19.0504	19.056
66	8.47576	-0.622776	3.18771	19.0501	19.0551	19.06	19.0648
67	8.50225	-0.614744	3.12265	19.0607	19.0651	19.0693	19.0735
68	8.52618	-0.606661	3.05857	19.0711	19.0748	19.0785	19.0821
69	8.54754	-0.598529	2.9954	19.0812	19.0843	19.0874	19.0905
70	8.56636	-0.59035	2.93309	19.0911	19.0937	19.0962	19.0987
71	8.58265	-0.582124	2.87158	19.1008	19.1028	19.1048	19.1068
72	8.59643	-0.573853	2.81083	19.1102	19.1117	19.1133	19.1148
73	8.60772	-0.56554	2.75078	19.1194	19.1205	19.1216	19.1227
74	8.61653	-0.557186	2.69139	19.1285	19.1291	19.1298	19.1304

θ_W (°)	u_0 (m/s)	v_0 (m/s)	δ_0 (°)	$\alpha_{0,1}$ (°)	$\alpha_{0,2}$ (°)	$\alpha_{0,3}$ (°)	$\alpha_{0,4}$ (°)
75	8.62287	-0.548792	2.63264	19.1373	19.1376	19.1379	19.1381
76	8.62653	-0.540317	2.57462	19.1461	19.146	19.1459	19.1458
77	8.62741	-0.531746	2.51735	19.1546	19.1543	19.1539	19.1535
78	8.62555	-0.523082	2.46078	19.1631	19.1624	19.1617	19.161
79	8.62098	-0.514327	2.40486	19.1714	19.1705	19.1695	19.1685
80	8.61372	-0.505484	2.34955	19.1796	19.1784	19.1772	19.1759
81	8.6038	-0.496554	2.29481	19.1877	19.1862	19.1847	19.1832
82	8.59125	-0.48754	2.24059	19.1956	19.1939	19.1922	19.1905
83	8.57611	-0.478446	2.18686	19.2035	19.2016	19.1997	19.1977
84	8.55841	-0.469273	2.13358	19.2113	19.2091	19.207	19.2048
85	8.53819	-0.460025	2.08071	19.219	19.2166	19.2143	19.2119
86	8.51547	-0.450704	2.02821	19.2266	19.2241	19.2215	19.219
87	8.49031	-0.441315	1.97606	19.2341	19.2314	19.2287	19.226
88	8.46273	-0.431858	1.92421	19.2415	19.2387	19.2358	19.2329
89	8.4328	-0.422336	1.87273	19.2489	19.2459	19.2429	19.2398
90	8.40082	-0.412741	1.8227	19.2562	19.253	19.2498	19.2465
91	8.3669	-0.403075	1.7744	19.2634	19.2601	19.2567	19.2533
92	8.33108	-0.39334	1.72785	19.2706	19.2671	19.2635	19.26
93	8.29342	-0.38354	1.68305	19.2776	19.274	19.2704	19.2666
94	8.25396	-0.373679	1.64	19.2846	19.2809	19.2771	19.2733
95	8.21276	-0.363761	1.59871	19.2916	19.2878	19.2839	19.2799
96	8.16987	-0.353789	1.55918	19.2985	19.2946	19.2906	19.2865
97	8.12534	-0.343767	1.52144	19.3054	19.3013	19.2972	19.2931
98	8.07923	-0.3337	1.4855	19.3122	19.3081	19.3039	19.2997
99	8.0316	-0.32359	1.45138	19.3189	19.3148	19.3105	19.3062
100	7.9825	-0.313442	1.41902	19.3257	19.3214	19.3171	19.3128
101	7.93185	-0.303258	1.38658	19.3324	19.3281	19.3238	19.3193
102	7.87966	-0.293041	1.35323	19.3392	19.3348	19.3304	19.3259
103	7.826	-0.282794	1.31893	19.3459	19.3415	19.337	19.3325
104	7.77091	-0.272522	1.28363	19.3526	19.3481	19.3436	19.339
105	7.71447	-0.262225	1.24731	19.3593	19.3548	19.3502	19.3456
106	7.65675	-0.251909	1.20993	19.3661	19.3615	19.3569	19.3522
107	7.5978	-0.241576	1.17143	19.3728	19.3682	19.3635	19.3588
108	7.53769	-0.231229	1.13177	19.3796	19.3749	19.3702	19.3653
109	7.47647	-0.22087	1.09096	19.3864	19.3817	19.3768	19.372
110	7.41373	-0.210503	1.05041	19.3933	19.3885	19.3836	19.3787
111	7.34929	-0.200127	1.01082	19.4001	19.3953	19.3904	19.3855
112	7.28324	-0.189745	0.972212	19.4071	19.4022	19.3973	19.3923
113	7.21565	-0.179354	0.934586	19.414	19.4091	19.4042	19.3992
114	7.14661	-0.168955	0.897966	19.421	19.4161	19.4111	19.4061
115	7.0762	-0.158547	0.862372	19.4281	19.4231	19.4181	19.4131
116	7.0045	-0.14813	0.827828	19.4352	19.4302	19.4252	19.4201
117	6.93183	-0.137811	0.793506	19.4424	19.4373	19.4323	19.4271
118	6.85866	-0.127781	0.757945	19.4496	19.4445	19.4394	19.4342
119	6.78507	-0.118042	0.721071	19.4568	19.4517	19.4465	19.4413
120	6.71112	-0.108595	0.682831	19.4642	19.459	19.4538	19.4485
121	6.63689	-0.0994384	0.643168	19.4716	19.4663	19.461	19.4557
122	6.56243	-0.0905715	0.602024	19.4791	19.4738	19.4684	19.463
123	6.48774	-0.0819426	0.55933	19.4867	19.4813	19.4758	19.4704
124	6.41265	-0.0734036	0.514986	19.4944	19.4889	19.4834	19.4779
125	6.33721	-0.0649421	0.468899	19.5022	19.4966	19.491	19.4854
126	6.26147	-0.0565539	0.420968	19.5101	19.5044	19.4988	19.4931
127	6.18551	-0.0482343	0.371086	19.5182	19.5124	19.5066	19.5008
128	6.10929	-0.0399734	0.319322	19.5264	19.5205	19.5146	19.5087
129	6.03193	-0.0317169	0.267685	19.5347	19.5287	19.5227	19.5168

θ_W (°)	u_0 (m/s)	v_0 (m/s)	δ_0 (°)	$\alpha_{0,1}$ (°)	$\alpha_{0,2}$ (°)	$\alpha_{0,3}$ (°)	$\alpha_{0,4}$ (°)
130	5.95322	-0.0234387	0.21673	19.5433	19.5372	19.5311	19.525
131	5.87319	-0.0151235	0.166434	19.5521	19.5459	19.5396	19.5334
132	5.79185	-0.00675298	0.116775	19.5611	19.5547	19.5484	19.5421
133	5.71062	0.00156629	0.0677808	19.5703	19.5638	19.5572	19.5508
134	5.63315	0.00951478	0.0196086	19.5796	19.5728	19.5661	19.5595
135	5.55935	0.0170898	-0.027665	19.5889	19.582	19.5751	19.5683
136	5.48899	0.0243054	-0.0739697	19.5984	19.5912	19.5842	19.5772
137	5.42169	0.031194	-0.119648	19.6079	19.6006	19.5934	19.5862
138	5.35618	0.0379389	-0.168268	19.6177	19.6102	19.6027	19.5954
139	5.29213	0.0445859	-0.220696	19.6278	19.62	19.6123	19.6047
140	5.22948	0.0511398	-0.276975	19.6382	19.63	19.6221	19.6142
141	5.16817	0.0576068	-0.337045	19.6488	19.6404	19.6321	19.624
142	5.10707	0.0640224	-0.397799	19.6598	19.651	19.6424	19.6339
143	5.04571	0.0704109	-0.457796	19.6713	19.662	19.653	19.6442
144	4.98407	0.0767842	-0.517047	19.6832	19.6735	19.664	19.6548
145	4.92218	0.0831587	-0.575577	19.6956	19.6854	19.6755	19.6659
146	4.86007	0.0896259	-0.633822	19.7086	19.6978	19.6874	19.6773
147	4.79772	0.0962373	-0.692014	19.7221	19.7107	19.6997	19.6891
148	4.73512	0.103009	-0.750163	19.7364	19.7243	19.7126	19.7015
149	4.67216	0.109926	-0.808417	19.7513	19.7384	19.7261	19.7143
150	4.60828	0.116809	-0.867559	19.7671	19.7533	19.7402	19.7276
151	4.54335	0.123647	-0.927814	19.7838	19.769	19.7549	19.7415
152	4.47728	0.130462	-0.989305	19.8016	19.7857	19.7705	19.7562
153	4.41114	0.137325	-1.05708	19.8208	19.8036	19.7874	19.7721
154	4.3462	0.144317	-1.13751	19.8412	19.8226	19.8052	19.7887
155	4.28242	0.151441	-1.2312	19.8632	19.8429	19.824	19.8062
156	4.2195	0.158731	-1.33824	19.8868	19.8644	19.8437	19.8244
157	4.15598	0.166374	-1.45453	19.9123	19.8874	19.8644	19.8431
158	4.09146	0.174445	-1.57989	19.9401	19.9121	19.8864	19.8629
159	4.02584	0.182988	-1.71539	19.9706	19.9388	19.9101	19.8839
160	3.95899	0.19201	-1.866	20.0042	19.968	19.9354	19.9061

Table A.4: VPP results for nonlinear unstable hull

θ_W (°)	u_0 (m/s)	v_0 (m/s)	δ_0 (°)	$\alpha_{0,1}$ (°)	$\alpha_{0,2}$ (°)	$\alpha_{0,3}$ (°)	$\alpha_{0,4}$ (°)
32	5.84305	-0.915935	6.54473	18.1551	18.3562	18.5087	18.6283
33	5.97802	-0.912432	6.32341	18.2293	18.4046	18.5407	18.6494
34	6.10909	-0.90873	6.11643	18.295	18.4488	18.5707	18.6696
35	6.23636	-0.904843	5.92248	18.3537	18.4893	18.5988	18.6891
36	6.35992	-0.900777	5.74032	18.4065	18.5267	18.6253	18.7078
37	6.47987	-0.896541	5.56888	18.4542	18.5612	18.6504	18.7259
38	6.59627	-0.892141	5.40719	18.4977	18.5933	18.6741	18.7433
39	6.7092	-0.887581	5.2544	18.5375	18.6232	18.6966	18.76
40	6.81871	-0.882867	5.10975	18.5741	18.6512	18.7179	18.7762
41	6.92485	-0.878001	4.97255	18.608	18.6775	18.7383	18.7919
42	7.02758	-0.872985	4.84223	18.6395	18.7024	18.758	18.8074
43	7.12669	-0.867809	4.71824	18.6689	18.7261	18.777	18.8226
44	7.22221	-0.862472	4.60008	18.6963	18.7484	18.7952	18.8373
45	7.31417	-0.856979	4.48729	18.7221	18.7696	18.8126	18.8515
46	7.40262	-0.851329	4.37944	18.7464	18.7898	18.8293	18.8654
47	7.48759	-0.845526	4.27616	18.7692	18.809	18.8454	18.8788
48	7.56911	-0.839571	4.17711	18.7908	18.8273	18.8608	18.8918
49	7.6472	-0.833465	4.08199	18.8114	18.8448	18.8757	18.9044
50	7.7219	-0.827211	3.9905	18.8308	18.8616	18.8901	18.9167

θ_W (°)	u_0 (m/s)	v_0 (m/s)	δ_0 (°)	$\alpha_{0,1}$ (°)	$\alpha_{0,2}$ (°)	$\alpha_{0,3}$ (°)	$\alpha_{0,4}$ (°)
51	7.79321	-0.82081	3.90241	18.8494	18.8776	18.904	18.9287
52	7.86118	-0.814264	3.81748	18.8671	18.8931	18.9174	18.9403
53	7.92581	-0.807574	3.73549	18.884	18.9079	18.9305	18.9517
54	7.98713	-0.800743	3.65625	18.9003	18.9223	18.9431	18.9628
55	8.04516	-0.793772	3.57958	18.9158	18.9361	18.9554	18.9737
56	8.09991	-0.786663	3.50532	18.9308	18.9495	18.9673	18.9842
57	8.15139	-0.779419	3.43332	18.9452	18.9624	18.9789	18.9946
58	8.19964	-0.772041	3.36343	18.9591	18.975	18.9902	19.0047
59	8.24465	-0.764532	3.29554	18.9725	18.9871	19.0012	19.0147
60	8.28675	-0.756895	3.22926	18.9853	18.9987	19.0115	19.0239
61	8.32629	-0.749141	3.16421	18.9978	19.0098	19.0215	19.0328
62	8.36327	-0.741271	3.10032	19.0098	19.0207	19.0314	19.0417
63	8.39771	-0.733288	3.03752	19.0214	19.0313	19.041	19.0503
64	8.42961	-0.725196	2.97575	19.0328	19.0417	19.0504	19.0588
65	8.45898	-0.716997	2.91495	19.0438	19.0518	19.0595	19.0672
66	8.48584	-0.708693	2.85506	19.0545	19.0616	19.0686	19.0754
67	8.51019	-0.700289	2.79602	19.0649	19.0712	19.0774	19.0835
68	8.53205	-0.691786	2.7378	19.0751	19.0806	19.0861	19.0914
69	8.55143	-0.683188	2.68034	19.085	19.0898	19.0946	19.0992
70	8.56834	-0.674499	2.62358	19.0947	19.0988	19.1029	19.107
71	8.5828	-0.665721	2.5675	19.1042	19.1077	19.1111	19.1146
72	8.59482	-0.656858	2.51204	19.1134	19.1163	19.1192	19.1221
73	8.60442	-0.647913	2.45717	19.1225	19.1249	19.1272	19.1295
74	8.61161	-0.63889	2.40285	19.1314	19.1332	19.135	19.1368
75	8.61641	-0.629792	2.34903	19.1401	19.1414	19.1428	19.1441
76	8.61876	-0.620608	2.29575	19.1487	19.1496	19.1505	19.1514
77	8.61842	-0.611289	2.24314	19.1572	19.1577	19.1582	19.1586
78	8.61538	-0.601837	2.19117	19.1655	19.1656	19.1658	19.1659
79	8.60968	-0.592254	2.1398	19.1737	19.1735	19.1733	19.173
80	8.60134	-0.582543	2.089	19.1818	19.1813	19.1807	19.1801
81	8.59039	-0.572709	2.03871	19.1898	19.1889	19.188	19.1871
82	8.57686	-0.562753	1.98891	19.1977	19.1965	19.1953	19.1941
83	8.56079	-0.552681	1.93956	19.2055	19.204	19.2025	19.201
84	8.54221	-0.542496	1.89063	19.2132	19.2114	19.2097	19.2079
85	8.52116	-0.532201	1.84208	19.2208	19.2188	19.2168	19.2148
86	8.49766	-0.5218	1.79388	19.2283	19.2261	19.2238	19.2216
87	8.47176	-0.511298	1.746	19.2358	19.2333	19.2308	19.2283
88	8.44351	-0.500697	1.69841	19.2432	19.2405	19.2378	19.2351
89	8.41293	-0.490003	1.65109	19.2505	19.2476	19.2447	19.2417
90	8.38027	-0.479208	1.60486	19.2577	19.2546	19.2515	19.2483
91	8.34573	-0.468311	1.56041	19.2649	19.2616	19.2582	19.2548
92	8.30936	-0.457316	1.51777	19.272	19.2685	19.2649	19.2613
93	8.27121	-0.446227	1.47691	19.279	19.2753	19.2716	19.2678
94	8.23132	-0.435048	1.43787	19.286	19.2821	19.2782	19.2743
95	8.18976	-0.423784	1.40064	19.2929	19.2889	19.2848	19.2807
96	8.14658	-0.412439	1.36525	19.2998	19.2956	19.2914	19.2871
97	8.10182	-0.401018	1.3317	19.3066	19.3023	19.2979	19.2935
98	8.05554	-0.389526	1.30001	19.3133	19.3089	19.3045	19.2999
99	8.00782	-0.377969	1.27022	19.3201	19.3155	19.311	19.3063
100	7.95868	-0.366347	1.24232	19.3268	19.3221	19.3175	19.3127
101	7.90807	-0.354666	1.21468	19.3334	19.3287	19.324	19.3191
102	7.85599	-0.342929	1.18614	19.3401	19.3353	19.3305	19.3256
103	7.80247	-0.331139	1.15668	19.3468	19.3419	19.337	19.332
104	7.7476	-0.319302	1.12627	19.3535	19.3485	19.3435	19.3384
105	7.69142	-0.30742	1.09486	19.3602	19.3551	19.35	19.3448

θ_W (°)	u_0 (m/s)	v_0 (m/s)	δ_0 (°)	$\alpha_{0,1}$ (°)	$\alpha_{0,2}$ (°)	$\alpha_{0,3}$ (°)	$\alpha_{0,4}$ (°)
106	7.63401	-0.295497	1.06243	19.3669	19.3617	19.3565	19.3512
107	7.57543	-0.283538	1.02892	19.3736	19.3684	19.3631	19.3577
108	7.51575	-0.271546	0.994309	19.3803	19.375	19.3696	19.3641
109	7.45502	-0.259523	0.958581	19.3871	19.3816	19.3762	19.3706
110	7.39283	-0.247474	0.923134	19.3939	19.3884	19.3828	19.3772
111	7.32899	-0.235399	0.888722	19.4007	19.3952	19.3895	19.3839
112	7.26359	-0.223299	0.855365	19.4076	19.402	19.3963	19.3906
113	7.19671	-0.211175	0.823083	19.4145	19.4088	19.4031	19.3973
114	7.12842	-0.199026	0.791901	19.4214	19.4157	19.4099	19.4041
115	7.05881	-0.186852	0.761846	19.4284	19.4227	19.4168	19.411
116	6.98796	-0.174652	0.732948	19.4355	19.4297	19.4238	19.4179
117	6.91619	-0.162561	0.70427	19.4426	19.4367	19.4308	19.4248
118	6.84394	-0.150796	0.674269	19.4497	19.4438	19.4378	19.4317
119	6.77129	-0.139363	0.642874	19.4569	19.4509	19.4448	19.4387
120	6.69828	-0.128261	0.610033	19.4642	19.4581	19.4519	19.4457
121	6.625	-0.117491	0.575693	19.4715	19.4653	19.4591	19.4528
122	6.55149	-0.107054	0.539795	19.479	19.4727	19.4663	19.46
123	6.47775	-0.0968829	0.502307	19.4865	19.4801	19.4737	19.4672
124	6.40361	-0.0868089	0.463234	19.4941	19.4876	19.4811	19.4746
125	6.32914	-0.0768197	0.422495	19.5018	19.4952	19.4886	19.482
126	6.25439	-0.0669108	0.379997	19.5097	19.503	19.4962	19.4895
127	6.17942	-0.0570775	0.335644	19.5177	19.5108	19.5039	19.4971
128	6.10419	-0.0473081	0.289543	19.5258	19.5188	19.5118	19.5048
129	6.02784	-0.0375391	0.243752	19.5341	19.5269	19.5198	19.5127
130	5.95016	-0.0277417	0.198808	19.5425	19.5353	19.528	19.5208
131	5.87119	-0.0178986	0.15471	19.5512	19.5438	19.5364	19.529
132	5.79094	-0.00798975	0.111462	19.5601	19.5525	19.5449	19.5374
133	5.71083	0.00185786	0.0690206	19.5692	19.5614	19.5536	19.5459
134	5.63439	0.0112698	0.0272856	19.5783	19.5703	19.5623	19.5545
135	5.56155	0.0202423	-0.013687	19.5875	19.5793	19.5711	19.5631
136	5.49208	0.0287889	-0.0538237	19.5968	19.5883	19.58	19.5717
137	5.4256	0.0369486	-0.0934297	19.6063	19.5975	19.5889	19.5805
138	5.36089	0.0449316	-0.135847	19.6159	19.6069	19.598	19.5894
139	5.29762	0.0527946	-0.181957	19.6258	19.6165	19.6073	19.5984
140	5.23572	0.0605443	-0.23181	19.636	19.6263	19.6169	19.6077
141	5.17515	0.0681826	-0.28536	19.6464	19.6364	19.6266	19.6171
142	5.11486	0.07575	-0.339672	19.6572	19.6468	19.6366	19.6267
143	5.05431	0.0832738	-0.393079	19.6684	19.6575	19.6469	19.6366
144	4.99349	0.0907704	-0.445604	19.6801	19.6686	19.6575	19.6468
145	4.93241	0.0982529	-0.497228	19.6922	19.6802	19.6686	19.6574
146	4.87111	0.105821	-0.548271	19.7049	19.6922	19.68	19.6683
147	4.80961	0.113536	-0.598911	19.7181	19.7047	19.6919	19.6797
148	4.74789	0.121416	-0.649138	19.7319	19.7178	19.7043	19.6914
149	4.68588	0.129455	-0.699031	19.7464	19.7314	19.7171	19.7036
150	4.623	0.137449	-0.749486	19.7617	19.7457	19.7305	19.7161
151	4.5591	0.145363	-0.800788	19.7778	19.7607	19.7446	19.7293
152	4.49409	0.153218	-0.853017	19.795	19.7766	19.7593	19.743
153	4.42869	0.161076	-0.909613	19.8134	19.7937	19.7752	19.7579
154	4.36449	0.169039	-0.977901	19.833	19.8118	19.792	19.7736
155	4.30142	0.177115	-1.05866	19.8541	19.831	19.8098	19.79
156	4.23938	0.185313	-1.15227	19.8766	19.8515	19.8283	19.807
157	4.17705	0.193817	-1.25482	19.9008	19.873	19.8476	19.8243
158	4.11383	0.202728	-1.36509	19.9271	19.8961	19.8681	19.8426
159	4.04962	0.212078	-1.48394	19.9558	19.921	19.8898	19.8618
160	3.98434	0.221876	-1.61435	19.9872	19.948	19.9131	19.8821